Ceramics International 51 (2025) 36777–36789

Contents lists available at ScienceDirect

Ceramics International

journal homepage: www.elsevier.com/locate/ceramint

Vitrification paths in porcelain Stoneware: Dependence on bulk chemical composition and effect on sintering behaviour

Sonia Conte [a,*], Chiara Molinari [a], Matteo Ardit [b], Daniele Giordano [a,c], Michele Dondi [a], Chiara Zanelli [a]

[a] CNR-ISSMC, Institute of Science, Technology and Sustainability for Ceramics, Via Granarolo 64, 48018, Faenza, Italy
[b] Department of Geosciences, University of Padova, Via G. Gradenigo 6, 35131, Padova, Italy
[c] Earth Sciences Department, University of Torino, Via Valperga Caluso 35, 10125, Torino, Italy

ARTICLE INFO

Handling Editor: Dr P. Vincenzini

Keywords:
Porcelain stoneware
Chemical composition
Phase transformation
Sintering behaviour

ABSTRACT

This study investigates the vitrification paths of porcelain stoneware, focusing on how bulk chemical compositions can influence sintering behaviour. In particular, leveraging the largest compositional database ever analysed in this context, the research aims to understand how the chemistry of ceramic bodies can influence phase transformations during the firing and thus the properties of the liquid phase at high temperatures. Porcelain stoneware compositions analysed were classified according to their alumosity – defined as the ratio of alumina to the sum of alumina and total flux oxides – and silica content. Four distinct compositional fields were identified: meta-aluminous, moderately peraluminous, frankly peraluminous, and strongly peraluminous. Each category exhibits specific vitrification paths, i.e., the nature, rate and extent of phase reactions that determine the amount and composition of the liquid phase at high temperature, and sintering behaviours. The study emphasizes the complex relationship between batch composition, phase evolution, and sintering kinetics. It demonstrates how variations in alumosity impact liquid phase development and characteristics, affecting key factors such as viscosity, surface tension, and densification efficiency. This comprehensive analysis offers new insights into porcelain stoneware manufacturing and introduces a predictive approach to batch formulation that complements conventional technological assessments. The findings hold significant potential to improve the design and optimization of porcelain stoneware compositions in industrial applications.

1. Introduction

Porcelain stoneware is a highly vitrified material with about 60–70 wt% vitreous phase, characterized by a compact microstructure with very low water absorption after fast firing at around 1200 °C [1,2]. It is the most popular body in the manufacture of ceramic tiles and slabs, both glazed and unglazed, all over the world [3]. This fact and the considerable versatility of the tile-making process, especially in terms of batch design, has enabled the use of various raw materials – beyond ball clay, kaolin, feldspar and quartz which constitute the basic ingredients of porcelain stoneware – and has become a common practice among manufacturers to mitigate cost and supply risks in body formulation [1,4,5]. This has led to a plethora of local variants, depending on the strategy of manufacturers (often a trial-and-error approach) and the features of the available raw materials, so that the compositional perimeter of porcelain stoneware has substantially expanded without a clear conceptualized approach [6].

Apparently, regardless of compositional variability, porcelain stoneware rapidly densifies by progressive wetting of residual and newly formed crystals (e.g., quartz, mullite, and feldspar) through the formation of an abundant liquid phase of meta-aluminous to slightly peraluminous composition. This is a distinctive trait for porcelain stoneware with industrial firing schedules typically last 40–70 min at maximum temperature of 1180–1220 °C, *versus* porcelain, which needs to be fired at higher temperature and for longer time to overcome the barrier to mullite crystal growth [7,8].

The phase evolution during the firing of porcelain stoneware tiles has been investigated in detail [5,9–15]. These studies have led to a better understanding of the mechanisms governing viscous flow sintering, in particular the kinetics and efficiency of densification as a function of the evolution of the chemico-physical properties of the melt at high temperature [16–18]. Consequently, it is crucial to characterize the

* Corresponding author.
E-mail address: sonia.conte@issmc.cnr.it (S. Conte).

https://doi.org/10.1016/j.ceramint.2025.05.388
Received 15 April 2025; Received in revised form 22 May 2025; Accepted 27 May 2025
Available online 27 May 2025

relationship between these physical properties and the composition of the liquid phase, as the latter depends on the melting of pre-existing mineral phases and the formation of newly formed crystals [8,13,18–20].

Attempts have been made to predict the firing behaviour of porcelain stoneware in a more or less wide compositional window by means of statistical approaches. The resulting models – taking into account the variability of batch composition [11,13] or based on microstructural constraints [21] – are essentially aimed at designing the batch in mineralogical terms, with the exception of recent studies based on oxide ratios [e.g. 22]. However, although the relationship between chemical composition and technological properties in silicate ceramics is well known, limited attention has been paid to constraining the effect of the chemistry of porcelain stoneware batches [19,22–25]. In fact, chemical composition has not yet entered industrial practice as a tool for batch design, apart from subjective considerations on the amount of alumina or fluxing agents (Na_2O, K_2O, CaO, MgO) and careful control of the body colour by checking the amount of Fe_2O_3 and TiO_2 [13,26].

In this study we aim to explore the range of chemical compositions of porcelain stoneware to gain a deeper understanding of how the phase reactions that occur during firing are influenced by the overall batch composition. Our objective is to uncover a potential correlation between the vitrification path (the nature, rate and extent of phase reactions that determine the quantity and composition of the liquid phase at high temperature) and the technological behaviour of bodies, with a particular focus on ceramic tiles.

Although, as mentioned above, batch design is typically carried out on a trial-and-error basis, both the tile-making process and the technological plants are globally standardized [3]. In industrial practice, this standardization constrains several important variables — such as particle size distribution, green bulk density, and firing schedule [27–31] — and facilitates the comparison of a wide range of bodies. We believe it is essential to define the compositional perimeter of porcelain stoneware on a non-empirical basis, using cause-and-effect relationships to provide feedback as guidelines for body formulation.

The aim of this contribution is to characterize the vitrification paths along with the evolution of key melt properties (e.g., viscosity, surface tension and chemistry described through pseudo-structural parameters) for a wide range of porcelain stoneware compositions. This analysis will determine whether varying body compositions predictably influence sintering behaviour.

2. Experimental rationale

The rationale of the present study is based on the following steps:

i) select various batch compositions, representative of the wide range of porcelain stoneware, complying with the standard requirement (water absorption $\leq$0.5 % according to ISO 13006, achieved with a firing temperature below 1240 °C and a cold-to-cold firing cycle of about 1 h);
ii) use available literature data on phase composition to follow phase transformations during firing as a function of batch composition;
iii) infer the properties of the melt (chemical composition and pseudo-structural parameters) as a function of the batch composition;
iv) draw vitrification paths occurring during the firing process, identifying the compositional perimeter of porcelain stoneware in the Na_2O-K_2O-Al_2O_3-SiO_2 diagram and discriminating fields with different phase evolution and liquid phase properties;
v) verify the extent to which different vitrification paths can affect the sintering behaviour.

Thirty-six batch compositions were selected from the literature on porcelain stoneware, for which both quantitative data on chemical and phase composition (for both unfired and fired bodies) and a full characterization of the sintering behaviour were available [8,18,32–39]. In addition, unpublished data of thirteen industrial batches (from authors' database) were considered. A further eighteen samples were selected for which no sintering data were available [15,40–44]. Details of the selected samples can be found in Table S1 (supplementary material). Moreover, for representative purposes, details on the goodness of a Rietveld refinement of a quantitative mineralogical analysis already published in one of our previous papers [39] and a selected XRPD pattern are shown in Fig. 1S (supplementary materials).

Phase transformations were assessed by considering the content of residual minerals and new formed phases after firing and their variation with respect to the raw batch (quartz, feldspars). For mullite, a mullitisation index was calculated by assuming firing reactions involving both kaolinite and illite, as reported in Table S2 (supplementary material).

Both the chemical and phase compositions were used to calculate the chemical composition of the liquid phase, also referred to as *melt* when at high temperature or as *vitreous phase* at room temperature (the *amorphous phase* refers to the non-crystalline components present around 1000 °C, before a liquid phase has formed). The methodology followed the approach of Conte et al. [45], which consists of subtracting the contribution of each mineralogical phase (taking into account its stoichiometric formula) from the bulk chemistry and normalising to 100 %. The mullite stoichiometry was determined by the unit cell *a*-axis, which length scales linearly with the amount of Al_2O_3 [18,46]. Details are reported in Table S2 (supplementary material).

The resulting chemical composition of the liquid phase was used to calculate pseudo-structural parameters: NBO/T, i.e. the amount of Non-Bridging Oxygens per Tetrahedrally coordinated cation [47]; the Glass Network Formers (GNF), Glass Network Modifiers (GNM) and Charge Compensators of Aluminium in Tetrahedral coordination, CCAT [34,48], as given in Table S2 (supplementary material). STAF empirical parameter was also computed. The chemical composition and pseudo-structural parameters of the liquid phase of all samples are reported in Table S3 (supplementary material).

The data are plotted in the Na_2O_{eq}-Al_2O_3-SiO_2 diagram, which is representative of almost the entire chemical composition of standard porcelain stoneware [6,34]. This modified phase diagram allows the contribution of potassium and alkali-earths oxides to be included in the Na_2O_{eq} parameter, calculated as the sum Na_2O + MgO + CaO + K_2O, having care to express the data as Na_2O equivalents using the following molar ratios: 1.538 (MgO), 1.105 (CaO), 0.658 (K_2O). The ternary diagram was transposed in the binary plot (Fig. 1): alumosity, $Al_2O_3/(Al_2O_3+Na_2O_{eq})$, *versus* silica (calculated on a dry basis, *i.e.,* normalized to 100 % without loss on ignition). Alumosity values of the batches are given in Table S1 and those of the liquid phases in Table S3, supplementary materials.

The phase transformation results were processed as contour maps in the silica-alumosity binary plot by Origin software (layer boundary; total points increase factor 100; smoothing parameter from 0.1 to 0.9).

The physical properties of the liquid phase at high temperature were estimated by predictive models based on the chemical composition of the liquid phase. The shear viscosity was calculated by the GRD model [49], while the effective viscosity of the body (ηeff) was calculated as the product of the shear viscosity of the melt (ηmelt) by the relative viscosity (ηrel), *i.e.,* ηeff = ηrel × ηmelt [18,34]. The relative viscosity was estimated by the relation: $\eta rel = [1-(\phi/\phi m)]^{-B\phi m}$, where ϕ is the solid load, ϕ_m is the critical fraction (set to 0.72) and *B* is the Einstein constant (*i.e., B* = 2.5) [50]. Table S3 also reports the calculated values of the liquid-vapor surface tension according to the Appen and Dietzel methods [45]. A sintering timescale (τ_s) was calculated as the ratio between melt viscosity and particle radius to surface tension [51]. These data are reported in Table S3 (supplementary material).

Key sintering parameters were inferred from isothermal densification curves. These include the temperature at which densification starts;

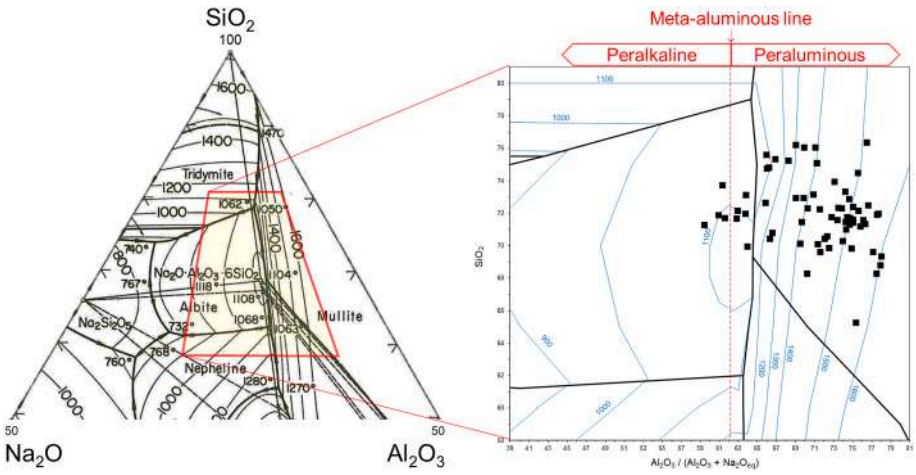

Fig. 1. Chemical composition of samples in the Na_2O_{eq}-Al_2O_3-SiO_2 ternary diagram (A) transposed in the alumosity [$Al_2O_3/(Al_2O_3+Na_2O_{eq})$] *versus* silica binary plot (B).

the initial sintering rate (for the neck formation stage); the total sintering rate; the effective viscosity of the ceramic body; the densification efficiency; and the bloating rate. The data necessary to calculate the above parameters were obtained by optical dilatometry (at temperatures in the range 1100–1250 °C) and He-pycnometry (to determine relative density) according to Conte et al. [34] and details in Fig. 2S (supplementary material).

3. Results and discussion

3.1. Phase transformations during firing

The variation in phase composition is hereafter represented as contour maps (rendered by a colour scale) as a function of batch alumosity and silica concentration, as we would like to show trends in phase changes as a function of $Al_2O_3/(Al_2O_3+Na_2O_{eq})$ and SiO_2 content. In any case, Fig. 3S is also reported in the supplementary materials, which shows the trends of mullite, feldspars and vitreous phase as a function of alumosity and quartz as a function of silica content (with correlation coefficient R^2).

The amount of **mullite** varies proportionally with batch alumosity, with no significant influence by the silica content (Fig. 2A). It ranges from less than 5 % for meta-aluminous batches to more than 10 % for markedly peraluminous formulations, in agreement with the literature [19,20,52–55 among others]. Interestingly, this trend is not only due to the increase in alumina, but also to the degree of mullitisation (i.e., the efficiency with which Al_2O_3 contained in kaolinite and illite is converted into mullite and this latter is preserved at the end of firing). The mullitisation index, which is less than 0.2 in meta-aluminous and weakly peraluminous batches, increases to over 0.5 in frankly peraluminous formulations with alumosity >71, coherently with the fact that mullite is unstable in the peralkaline field (Fig. 2B). The degree of mullitisation, as here calculated, cannot be directly compared with previous studies using different equations [23,25]. However, a good match was found when the literature data could be recalculated [11–13,25,56–59]. There also seems to be a relationship with silica concentration, with mullitisation being maximum in the range of 70–73 % SiO_2 for alumosity >71 %. This picture is undoubtedly influenced by various factors such as the crystallinity of kaolinite, particle size, extent of mixing, and interaction with the melt [2,30,60–63].

In principle, the amount of **quartz** remaining after firing varies in proportion to the silica concentration in the batch (Fig. 3A). For silica concentrations above 75 %, the residual quartz content exceeds 24 %, while for SiO_2 concentrations below 71 %, the quartz content is generally less than 21 %.

To a first approximation, these values correspond to the average quartz content in porcelain stoneware [19,64]. In detail, however, fields of different quartz content lie on sub-horizontal bands, indicate a slight decrease in quartz with increasing alumosity. In addition, this trend is broken in an oblique field (which includes both meta-aluminous and weakly peraluminous formulations relatively poor in silica) where moderate quartz contents (15–18 %) occur. This anomaly reflects the peculiar pattern of the degree of quartz dissolution, i.e. the percentage that is melted during firing compared to the initial quartz content (Fig. 3B). The dissolution degree is higher in the most peraluminous formulations, where it can exceed 30 %, which explains the inclination of the fields in Fig. 3A, in good agreement with previous studies [25, 56–59]. On the other hand, quartz seems to be more stable in

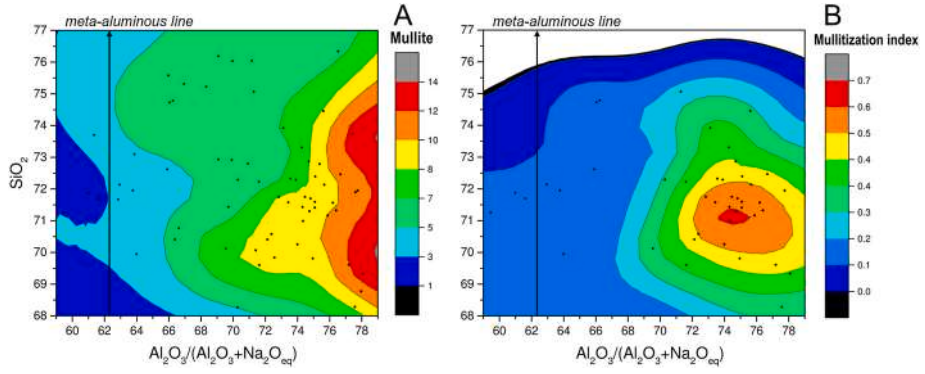

Fig. 2. Contour map of mullite content (wt%) (A) and mullitisation index (B) in the alumosity *vs*. silica diagram (black dots = samples).

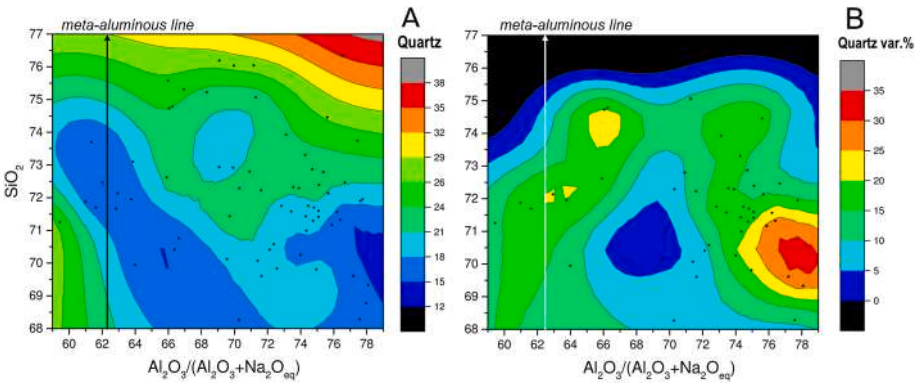

Fig. 3. Contour map of quartz (A) and degree of quartz dissolution (B) in the alumosity *vs.* silica diagram (black dots = samples).

moderately peraluminous and less siliceous batches, in agreement with literature models that predict a quartz dissolution of less than 10 % relative for fast firing cycles [11,65]. It should be noted that the use of glassy raw materials or some strong fluxes can induce a greater reactivity of quartz during firing [34,36,39,40,52,63,66–69].

The quantity of residual **feldspars** varies according to the alumosity and silica content of the batch. Under ceramic firing conditions, feldspars do not melt either by eutectic reaction with quartz or by incongruent reaction (K-feldspar = leucite + liquid), as known from previous studies [70]. At the meta-aluminous line and in relatively silica-poor and weakly peraluminous bodies, both plagioclase and K-feldspar occur up to 18 % (Fig. 4A) and up to 8 % (Fig. 4B), respectively. Both are almost absent in distinctly peraluminous formulations where the degree of dissolution of feldspars is in many cases greater than 90 %, while in batches with alumosity below 68 % the quantity of feldspar melted is generally less than 60 % (Fig. 4C). This is consistent with the literature, which mostly refers to peraluminous batches [11,25,56–59].

As feldspars are unstable in the peraluminous field, their residual content seems to be related not only to the increasing dissolution kinetics with increasing alumosity. In particular, high amounts of feldspars in the finished product may be due either to the persistence of the raw material in contact with peralkaline melts or to the crystallisation during firing of plagioclase (more or less calcic) and, exceptionally, anorthoclase or sanidine [9,35,67,69,71,72]. This explains the peak in the ratio of quartz to feldspar dissolved during firing, which is practically adjacent to the feldspar composition in the alumosity *vs.* silica diagram (Fig. 4D). While the ratio is below 0.3 in the rest of the diagram, it exceeds unity in this narrow compositional range, so that quartz appears to be dissolved more than feldspars.

The amount of **vitreous phase** varies moderately as a function of batch composition. As a matter of fact, most bodies fall within the 60–68 % range, with the highest values found in frankly peraluminous and silica-poor batches (Fig. 5A). These results are consistent with literature data [12,13,19,25,56–59]. At variance, the value of non-bridging oxygens per tetrahedrally-coordinated cation increases as a function of alumosity (Fig. 5B). The vitreous phase in meta-aluminous to weakly peraluminous bodies is strongly polymerized (NBO/T < 0.1), while that in peraluminous formulations is increasingly de-polymerized (up to

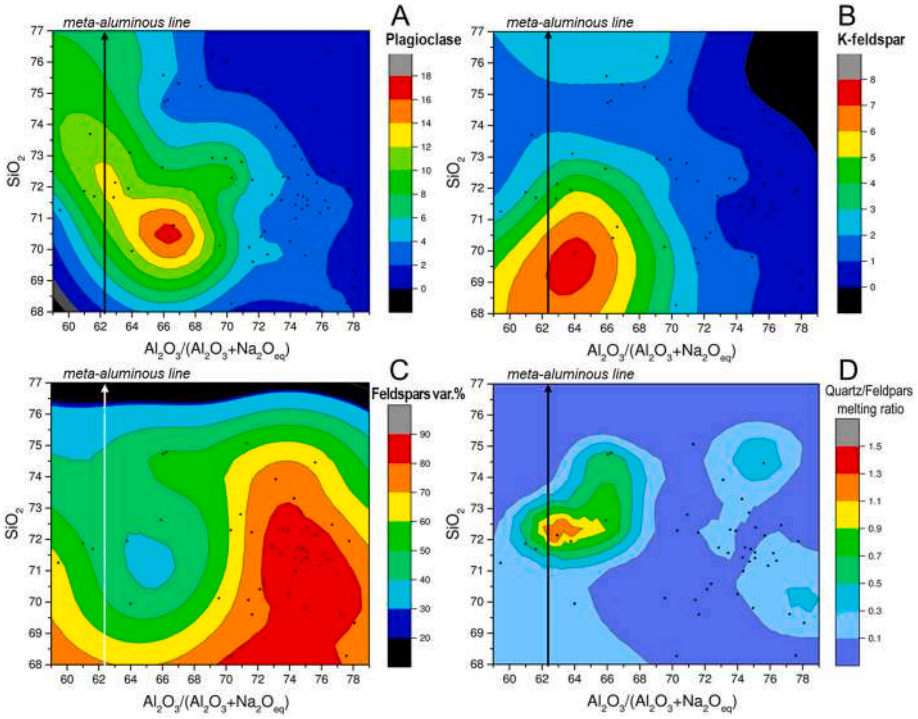

Fig. 4. Contour map of plagioclase (A), K-feldspar (B), degree of feldspars dissolution (C) and melted quartz-to-melted feldspars ratio (D) in the alumosity *vs.* silica diagram (black dots = samples).

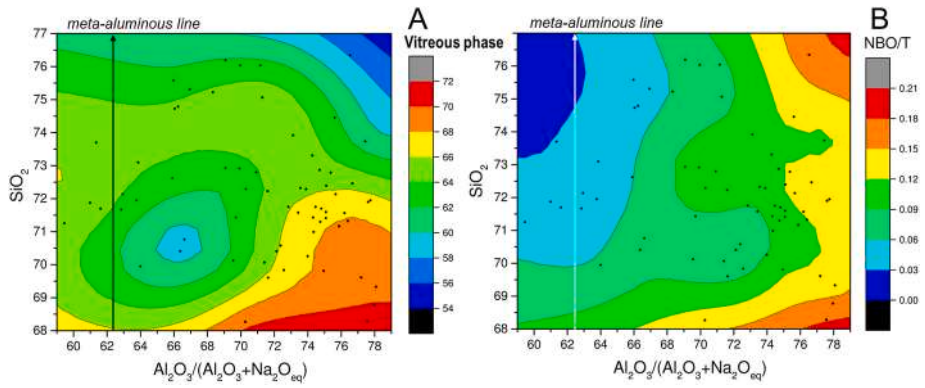

Fig. 5. Contour map of the vitreous phase (A) and its degree of de-polymerization as NBO/T (B) in the alumosity *vs*. silica diagram (black dots = samples).

NBO/T 0.5), as expected for such compositions [47,73].

3.2. Vitrification paths

The above observations help to delineate vitrification paths, i.e. how changes in the composition of the crystalline phases are reflected in the amount and composition of the liquid phase at high temperature [18,20]. Indeed, variations in the content of mullite, quartz, and feldspars appear to correlate with batch composition, as illustrated in Fig. 6, which shows the behaviour of representative porcelain stoneware samples with three different levels of aluminosity. These bodies were chosen because a comprehensive characterization is available over a wide range of firing temperatures [8]. Indeed, the evolution of the liquid phase composition depends on whether the batch is meta-aluminous (GSTO), moderately peraluminous (GPOR) or strongly peraluminous (POST), with distinct trends (Fig. 6A). The amount and composition of the liquid phase therefore reflect the contributions of the crystalline phases, which are progressively dissolved with increasing temperature [19,74–76].

Fig. 6B shows the contribution of feldspar, quartz and mullite crystalline phases to the vitrification path of the three porcelain stoneware bodies. The resultant of such a crystalline dissolution path substantially mirrors the phase evolution shown in Fig. 6C. In peraluminous batches, the amorphous phase around 1000 °C is essentially derived from clay minerals breakdown [8,34,37,76] and its composition depends on the efficiency with which the mullite formation takes place (or the mullitisation index). As the temperature increases, a liquid phase is formed from the melting of feldspars and quartz, so that the resultant vitrification path is somewhere in between the "vectors" of dissolution of these minerals (Fig. 6B). Interestingly, the contribution from mullite precipitation (in the peraluminous field) has a direction that is more or less the same as the feldspar "vector". In strongly peraluminous bodies, such as POST up to 1150 °C, the vitrification path initially lies beyond the glass formation boundary [76], implying a melt mixed with amorphous aluminous components. In moderately peraluminous batches, feldspars are much more involved in firing reactions than quartz. This is related to the ratio of melted fractions, which is lower in moderately peraluminous batches than in strongly peraluminous batches (i.e., on average quartz:feldspars ~1:8 and ~1:3, respectively).

The trend is different for meta-aluminous batches containing silicate glass as a raw material (e.g. GSTO). In these cases, the amorphous phase around 1000 °C originates not only from the clay minerals breakdown, but also from the soda-lime-silica glass itself, so that the non-crystalline composition is clearly peralkaline from the outset. Mullite, which is not stable in the peralkaline field, dissolves in the melt and contributes to the increase in alumosity with increasing temperature. Nevertheless, the trend remains almost sub-horizontal (i.e. a constant silica content) due to the simultaneous melting of quartz and feldspars (with a ratio close to unity).

It is therefore possible to identify distinct porcelain stoneware

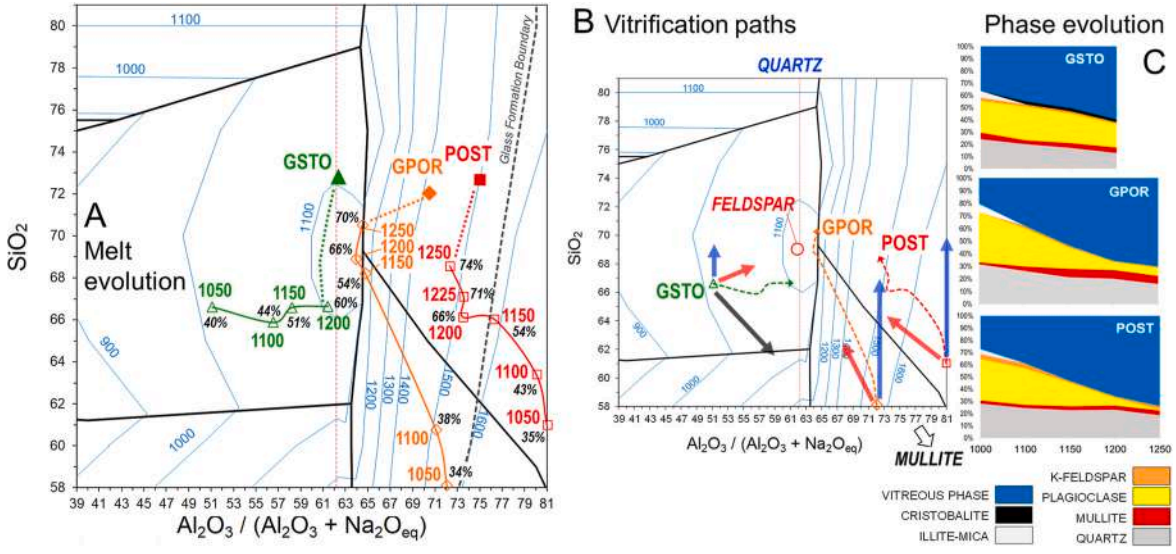

Fig. 6. Firing behaviour of three porcelain stoneware bodies with different alumosities: A) Melt evolution (amount and composition) as a function of temperature; B) Vitrification paths (arrows indicate the variation in melt composition as a consequence of quartz, feldspar or mullite dissolution); C) Evolution of phase composition as a function of temperature (modified after Conte et al. [8]).

batches, each characterized by specific ranges of alumosity and silica content, along with their unique vitrification paths (Fig. 7A). The batch composition can be correlated with that of the corresponding vitreous phase, which consistently exhibits lower silica content and lower alumosity compared to the respective batch (Fig. 7B). Based on this information, four compositional fields can be distinguished, arranged obliquely in the alumosity-silica diagram, each demonstrating comparable phase evolution and melt composition. Similar alignments of batch and melt compositions were noted by Owen and Dostal [77]. Consequently, these porcelain stoneware classes represent different vitrification paths (Fig. 7C), namely:

MAL: bodies with composition straddling the meta-aluminous line, resulting in peralkaline melts;

PAL1: moderately peraluminous bodies producing liquid phases close to the meta-aluminous line, ranging from slightly peralkaline (more siliceous than MAL melts) to slightly peraluminous (poorer in silica than the PAL2 melts);

PAL2: bodies with a frankly peraluminous character but producing liquid phases close to the vertical cotectic line, with a moderately peraluminous composition. As the compositional field crosses the cotectic, the most silica-rich melts are meta-aluminous, while those poorest in silica are more peraluminous;

PAL3: strongly peraluminous bodies (~79 % alumosity is the cut-off for porcelain-like batches, such as vitreous china, according to Conte et al. [6]) and the corresponding liquid phases are also strongly peraluminous.

These classes have been defined primarily to facilitate the presentation and discussion of the data in subsequent sections, as there is evidence of a gradual transition in the vitrification paths. Therefore, they are not intended to represent different product types within the porcelain stoneware assembly.

3.3. Composition and physical properties of the melt

Although the amount of vitreous phase deriving from the supercooling of the liquid matrix varies apparently without distinction between the classes of porcelain stoneware (see Fig. 5A), there are significant differences in the chemical composition which are related to the physical properties at high temperature. The duality in composition between bodies and melts may induce some confusion, since the target is to trace the observed behaviour back to the batch formulations, but to do this it is necessary to refer to the liquid phase, which always has a composition different from the body.

As shown in Fig. 7C, the melts tend to approach the composition of the equilibrium liquidus, as can be appreciated for most PAL1 and PAL2 bodies. This confirms what has been observed in previous feldspar melting experiments since the first few minutes [78]. This is not the case with melts formed in PAL3 batches, which are still in subliquidus at the optimal firing temperature for porcelain stoneware. In contrast, the liquid phase in MAL bodies appears to be above the liquidus surface, although this may only be apparent as these are relatively CaO- and MgO-rich melts for which the liquidus surface is expected to be at a higher temperature than that shown for alkaline systems.

All melt compositions fall within the glass formation boundary (GFB) for the Na_2O-Al_2O_3-SiO_2 system, which extends towards a more aluminous composition compared to the predominantly potassic porcelain bodies [76]. However, at a $Na_2O/(Na_2O + K_2O)$ ratio of 0.7, which is the mean value in porcelain stoneware melts, the GFB is considerably shifted towards lower alumosity and approximately half of the PAL3 melts, as well as some PAL2 and PAL1, lie beyond it (Fig. 7B). This fact explains why the most peraluminous batches must essentially be based on sodic fluxes. In addition, porcelain stoneware has stable melts up to a higher alumosity than porcelain and this can explain the different evolution of mullite [8,76].

Regarding the composition of the liquid phase, it is important to examine the pseudo-structural parameters, i.e. the glass network formers and modifiers, in terms of their constituent quantities and elements (Fig. 8). It is worth noting that these parameters are calculated from the chemistry of the liquid phase, which in turn is calculated from the chemistry of the body and its mineralogical composition after firing. This may imply some relative error in their calculation, which is why the following discussion will present these data from a perspective of

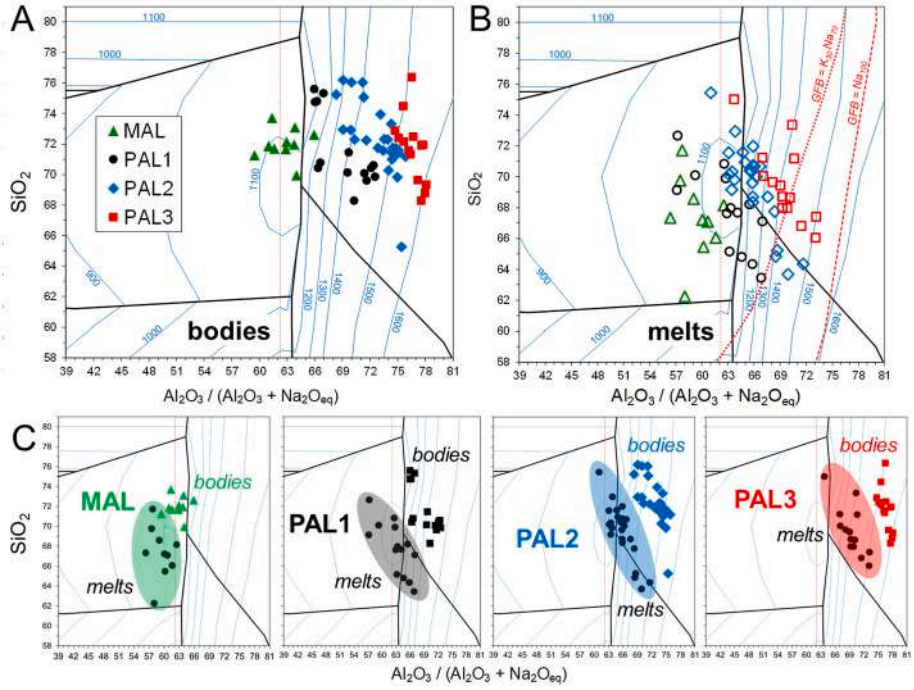

Fig. 7. Chemical composition of the bodies (A) and the corresponding vitreous phase (B) in the alumosity *vs.* silica diagram. Samples are rationalised into four classes based on chemical composition (C): meta-aluminous (MAL) or increasingly peraluminous (PAL1, PAL2, PAL3). GFB: Glass Formation Boundary for both the Na_2O-Al_2O_3-SiO_2 and $0.7Na_2O$-$0.3K_2O$-Al_2O_3-SiO_2 systems.

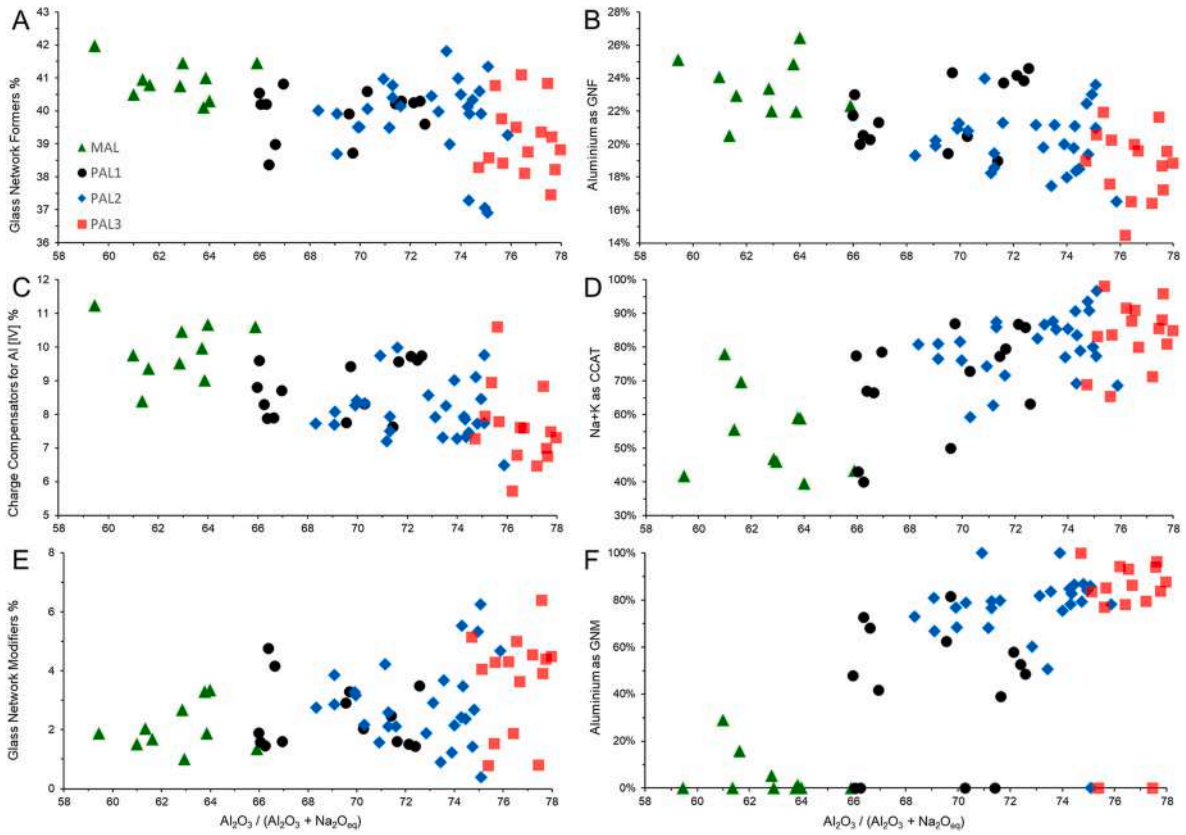

Fig. 8. Pseudo-structural parameters of the vitreous phase as a function of alumosity: (A) Glass Network Formers, GNF, (at%) and (B) percentage of aluminium as GNF; (C) Charge Compensators of Aluminium in Tetrahedral coordination, CCAT, (at%) and (D) sum of Na + K as CCAT (at%); (E) Glass Network Modifiers, GNM, (at %) and (F) percentage of aluminium as GNM. Relative error is within the symbol size.

gradual transitions between chemical classes, rather than rigid divisions.

Glass Network Formers (GNF) in porcelain stoneware are basically silicon and aluminium in tetrahedral coordination with oxygen, as the concentration of iron is usually very low. The amount of GNF is generally in the 37–42 at% range, which corresponds to a highly polymerized melt for MAL, PAL1 and PAL2 batches (Fig. 8A). A slight decrease is observed for the vitreous phase in PAL3 compositions, which is less polymerized. The most significant change is in the Si/Al ratio of GNF, with the percentage of Al decreasing progressively as the alumosity increases (Fig. 8B).

Charge Compensators (CCAT) are those alkaline and alkaline-earth elements that contribute to the incorporation of aluminium in tetrahedral coordination as glass network former. The amount of CCAT is in the 6–12 at% range, with a marked decrease with increasing alumosity (Fig. 8C). In parallel, the composition of CCAT changes, becoming more alkaline in peraluminous batches (Fig. 8D). This trend is explained to a large extent by the increased availability of sodium and potassium as a result of the more efficient dissolution of feldspars with increasing alumosity. Consequently, it is the availability of alkali that is crucial to achieve greater polymerization of the vitreous phase through the incorporation of aluminium into the glass tetrahedral network [48].

Glass Network Modifiers (GNM) vary widely in the 1–7 at% range, although a direct correlation with alumosity can be appreciated. Indeed, the GNM amount increases on average from MAL to PAL3 bodies (Fig. 8E). At the same time, there is a clear increase in the content of aluminium as GNM, which becomes prevalent in PAL2 and almost exclusive in PAL3 bodies (Fig. 8F). This is likely to have an implication on the physical characteristics of the melt: when the glass network is essentially modified by Al^{3+}, a different behaviour is expected compared to the case where the modifiers are alkalis and alkali-earths [48]. As the alumosity increases, there is a gradual change in the structural role of aluminium in the melt, from being mainly a GNF in meta-aluminous batches (MAL) to behaves equally as a GNF and GNM in strongly peraluminous batches (PAL3). This trend is expected and has been interpreted in terms of triclustered [79] or five-fold coordinated aluminium [80].

Physical properties of the melt at firing temperature were estimated for shear viscosity, liquid-gas surface tension and timescale (i.e., the ratio of viscosity by initial particle size to surface tension). These estimates are calculated cumulatively and compared for the various classes of porcelain stoneware (boxplots in Fig. 9) and provided individually for each sample in Table 3S (supplementary material).

The **shear viscosity** of the melt is in most cases between 3.8 and 5.3 $\log_{10}$ Pa·s at the maximum firing temperature, which is usually close to 1200 °C. A direct relationship between melt viscosity and batch alumosity clearly emerges (Fig. 9A). Evidence that viscosity of peraluminous melts is inversely correlated with the degree of alumosity [79,81–83] does not seem to have a significant effect on the estimate made with the GRD model (Fig. 4S) or an alternative model [84]. At most, a slight overestimation of viscosity may occur for the most peraluminous samples (in the order of 0.2–0.3 $\log_{10}$ Pa·s). Thus, the actual viscosity of the liquid phase in PAL3 bodies might be close to the values for PAL2 batches.

The **surface tension** of the liquid phase fluctuates in a narrow range, typically between 0.33 and 0.36 N m^{-1} at the maximum firing temperature. There seems to be an inverse relationship between surface tension and alumosity, as the mean values decrease from meta-aluminous (MAL batches) towards the peraluminous fields (Fig. 9B).

The **timescale** is lower in the meta-aluminous and slightly peraluminous compositions, as MAL and PAL1 batches typically have values in the 0.4–0.8 s range due to the lower viscosity and slightly higher surface tension of their melts. In contrast, frankly peraluminous

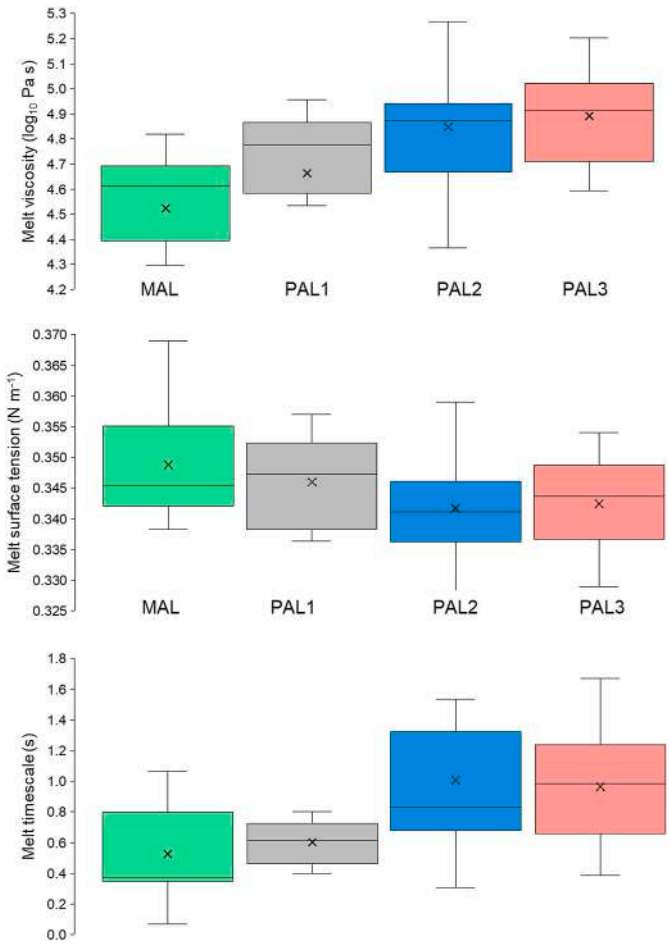

Fig. 9. Box-and-whisker plots of physical properties of the liquid phase at the specific temperature of maximum densification for each porcelain stoneware as alumosity increases: A) shear viscosity, B) gas-liquid surface tension, C) timescale.

compositions show a wider range of timescale, with most values between 0.7 and 1.4 s, but no significant difference between PAL2 and PAL3 bodies (Fig. 9C). The presumable overestimation of viscosity in the most peraluminous melts does not substantially affect the timescale of PAL3 with respect to PAL2 bodies.

Interestingly, the viscosity of the liquid phase in porcelain stoneware, as predicted by the GRD model, scales with an empirical parameter STAF, defined as the sum of $SiO_2 + aTiO_2 + bAl_2O_3 + cFeO_{tot}$, in molar percentage, where *a*, *b* and *c* are adjustable parameters. The parameters *a*, *b* and *c*, optimised for best scale viscosity and process timescales (and also to highlight the potential competition between iron and aluminium at tetrahedral sites), give the best STAF parameter when a = 1, b = ½, and c = −1. This is explained by the fact that the viscosity is primarily influenced by glass network formers, and therefore by the content of silica, and by the presence of cations that can be in four-fold coordination, e.g. Al^{3+} (with the charge mismatch compensated by CCAT) and to a certain extent iron and titanium, which have amphoteric behaviour in aluminosilicate melts.

The values obtained by this best-fit strategy seem to indicate that iron does not act as a network former and it also balances/buffers the role of Al as network former. STAF is positively correlated with the melt viscosity, particularly for compositions straddling the meta-aluminous line (Fig. 10A), and with the melt timescale, which accounts also for the surface tension (Fig. 10B). Therefore, STAF could be considered as a useful proxy for batch design once the phase transformations that occur during firing are taken into account.

3.4. Effect on sintering behaviour

Porcelain stoneware batches behave differently in the firing process, both in terms of kinetics (start of densification, sintering rates) and densification efficiency (Fig. 11). Another parameter of particular relevance for ceramic slabs is the dimensional stability at maximum temperature [85], which is inversely related to the bloating rate.

It has been suggested that the **start of densification** is somehow related to the critical liquid phase content, beyond which there is a rapid decrease in bulk viscosity that can trigger shrinkage [17,50]. This hypothesis has not been supported by experimental observations on porcelain stoneware, since very little data is available on the solid load present at the onset of densification (mostly between 940 and 1040 °C). Statistically, a clear increase in temperature is observed as alumosity increases, with the onset of densification averaging 951 ± 17 °C for meta-aluminous batches (MAL), 976 ± 12 °C for moderately peraluminous batches (PAL1) and 996 ± 19 °C for strongly peraluminous batches (PAL3). The data for the PAL2 population are more heterogeneous and the average is 1011 ± 55 °C (Fig. 11A).

The **initial sintering rate** refers to the neck formation stage, where there is a linear relationship between shrinkage and time [18,86,87]. The rates vary quite widely, mostly in the 1.8–3.5 min^{-1} range, with no clear relationship with the composition of bodies and glassy phases (Fig. 11B). This observation is unexpected, as the theory of sintering for glassy materials predicts that the rate of densification is inversely related to the melt timescale [86,87]. Instead, porcelain stoneware appears to proceed with densification once it reaches a critical condition (corresponding to a given timescale). This is consistent with the different temperature at which densification is triggered (lower in more reactive batches, which exhibit a faster timescale).

The **total sintering rate** is calculated cumulatively for both neck formation and vented bubble stages [86,87]. The densification kinetics

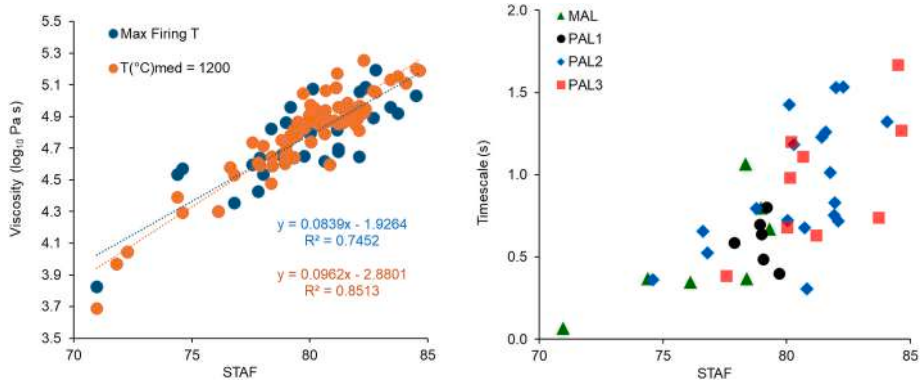

Fig. 10. Correlation of STAF with the melt viscosity (A) and melt timescale (B). Relative error is within the symbol size.

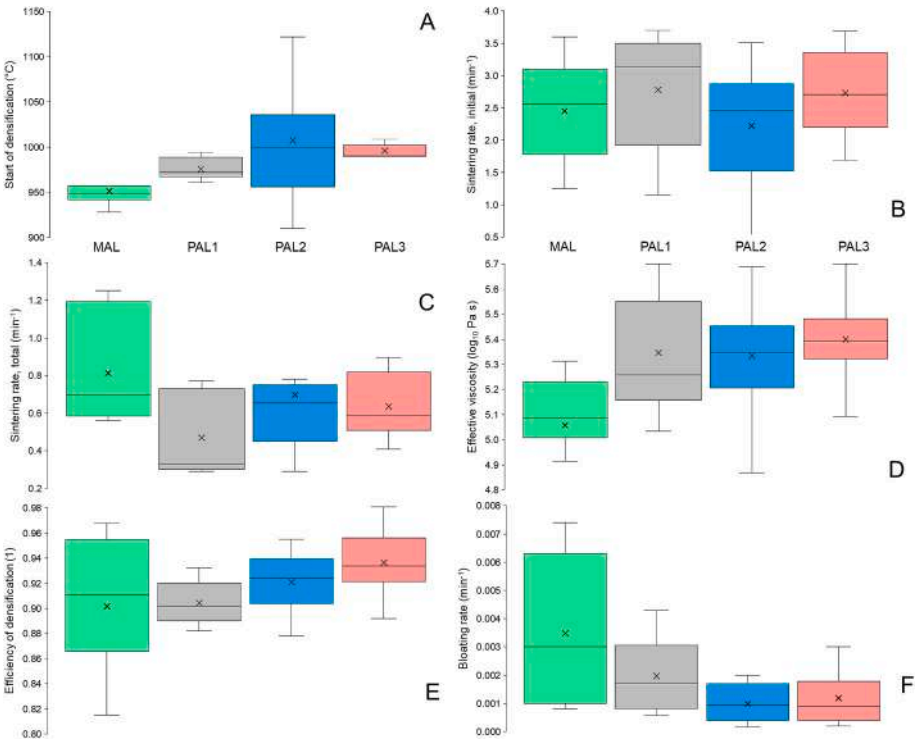

Fig. 11. Box-and-whisker plots of sintering parameters in porcelain stoneware as alumosity increases. A) Temperature at which densification starts; B) Sintering rate, initial (neck formation stage); C) Sintering rate (total); D) Effective viscosity; E) Efficiency of densification; F) Bloating rate.

is clearly differentiated between meta-aluminous batches on the one hand and peraluminous compositions on the other (Fig. 11C). On average, the MAL samples exhibit faster rates, mainly in the vented bubble stage, as peralkaline melts allow maximum density to be reached more rapidly. The peraluminous classes have broadly comparable sintering rates, although statistically there is some increase from PAL1 to PAL3. Although modest, this difference seems significant since it relates to the efficiency of densification. The expected inverse relationship between total sintering rate and melt viscosity (or timescale) can be glimpsed by comparing the mean values of the four classes.

Effective viscosity is the viscosity of the bulk ceramic body estimated from the viscosity of the liquid phase, taking into account the influence of the solid load through the relative viscosity [17,18]. This parameter is expected to influence the pyroplasticity and thus the dimensional stability of the tiles at the maximum firing temperature [32,88,89]. The effective viscosity in porcelain stoneware varies in a narrow range, mostly between 5.2 and 5.5 $\log_{10}$Pa·s in peraluminous batches, while in meta-aluminous batches the average value is lower and data are often below 5.2 $\log_{10}$Pa·s (Fig. 11D). This distinction is significant, beyond the apparently small difference, because a peculiar feature of porcelain stoneware is its ability to spontaneously dampen variations in effective viscosity. This phenomenon occurs through a kind of buffering effect, since the loss of solid load due to the dissolution of quartz at high temperature induces a reduction in effective viscosity, which is compensated by the silica increase in the liquid phase, which in turn boosts the melt viscosity [18,45]. Data suggest that this buffering action is effective in peraluminous formulations, especially when the phase composition is simpler and there are no more residual feldspars (PAL3). On the contrary, it is less effective in the presence of peralkaline melts, especially when residual or new formed feldspars are abundant and involved in the reactions that take place at dwell temperature (MAL).

Efficiency of densification is directly related to the batch alumosity and again the contrast between meta-aluminous and peraluminous batches is found (Fig. 11E). Considering the MAL samples, it emerges that starting the densification process earlier and carrying it out with faster kinetics (thanks to peralkaline melts) does not necessarily result in better densified products, but often the opposite. It should be noted that the residual porosity is on average higher in the MAL bodies and therefore the sintering rate results higher, also because the process is stopped earlier than in peraluminous formulations. The peraluminous bodies show a direct correlation between total sintering rate and efficiency of densification, with PAL3 batches densifying better on average than PAL2 and PAL1. This result is not consistent with the physical properties of the liquid phase (particularly the higher viscosity and the lower surface tension of PAL3 bodies). Nevertheless, it must be taken into account that the degree of densification is substantially affected by a trade-off between the sintering rate and the onset of overfiring phenomena, which have opposite effects. A faster densification process is more difficult to control and there is evidence that it is more easily reversed into bloating [18].

The **bloating rate** shows an inverse relationship with alumosity, with decreasing average values from MAL to PAL2 and then a slight increase for PAL3 (Fig. 11F). This ranking is consistent with the effective viscosity, as a cause-and-effect relationship is expected between bulk viscosity and pyroplasticity [32,45].

3.5. *Repercussions on batch design*

The fact that a gradual variation in the firing behaviour has been identified across the compositional perimeter of porcelain stoneware obviously has repercussions on batch design. The indications that emerge are of statistical value – based on the largest data set ever studied in detail for porcelain stoneware – and, as far as the properties of the melt at high temperature (such as viscosity) are concerned, based on models that in the peraluminous field seem to slightly overestimate the predictions. This aspect, in particular, will certainly need to be investigated further through experimental rheological analyses of the liquid phase at high temperature, coupled with structural spectroscopic analyses of these complex systems. Nevertheless, the obtained information framework is supported by a concatenation of cause-and-effect

relationships. In fact, it is possible to link the chemical and mineralogical composition of the batches to the phase transformations that occur during firing. From this standpoint, it is possible to identify vitrification paths that show how the composition of the liquid phase varies during firing. This information can be used to estimate the high temperature physical properties that govern the sintering, and then follow their effects on the firing behaviour through the HSM experimental determinations.

However, the technological constraints imposed by the production process of ceramic tiles and slabs cannot be avoided in batch design. For instance, the presence of a significant quantity of clay materials is unavoidable to provide the plasticity and other properties required in body preparation and tile pressing. This explains why porcelain stoneware batches are always peraluminous, although the alumosity degree depends on the clay materials used, as the alumina content decreases from high-grade kaolin to low-grade kaolin, kaolinitic ball clay, illite-kaolinite ball clay, bentonite and eventually further types [4]. Therefore, the main way to adjust batch alumosity is to tune the ratio between clay materials (e.g., kaolin versus ball clay). Another possible solution is to act on the flux side, even if feldspars and feldspathoids have the molar ratio $Al_2O_3/(Na_2O + K_2O + CaO) = 1$, so that their compositions always plot on the meta-aluminous line, even if they have different silica contents. A modest excess of alumina may occur in weathered fluxes, which may contain kaolinite, or in particular raw materials (granite, pegmatite, gneiss), which can be peraluminous due to accessory minerals (muscovite, cordierite, sillimanite, etc.). However, the most effective way of reducing the degree of alumosity is to use low alumina fluxes – natural (talc, chlorite, diopside, wollastonite, carbonates) or glassy (e.g., soda-lime-silica cullet) – instead of feldspathic raw materials. The use of peralkaline granite/rhyolite/syenite is generally not effective because the alkali excess is mostly due to mafic minerals (e.g., aegirine), which are removed as much as possible during raw material processing.

The indications referring to the chemical composition of the batches cannot be easily linked to their formulation in terms of raw materials or mineralogical composition. For instance, when the samples are plotted in the clay minerals-fluxes-quartz ternary diagram, the MAL and PAL classes appear to overlap to a large extent (Fig. 12A). Several samples belonging to all four classes fall within the white and super white porcelain stoneware [1]. However, other samples fall into the recently proposed field based on a microstructural design of the porcelain stoneware bodies [21]: these are mainly the PAL3 compositions (as well as some PAL2 and MAL). This supports the importance of assessing the degree of alumosity of the batches, which is in agreement with the recommendation to increase the content of kaolinite as a mullite precursor [21].

The approach followed in the present study also allows the ambivalent role of mullite to be highlighted, both from a microstructural point of view and as the main buffer of alumina. In fact, the alumina content of the melt (and therefore its viscosity) depends to a large extent on the dissolution-precipitation of mullite [8,13,18].

However, in order to describe the batch composition in mineralogical terms, it is necessary to overcome the ambiguity, particularly insidious in triaxial batches, that raw materials (clays, fluxes, silica sources) do not correspond exactly to the minerals (kaolinite + illite, feldspars, quartz).

In terms of batch design, the four classes of porcelain stoneware correspond to predictable variations in the ratio of raw materials, with a progressive decrease in average fluxes content and a parallel increase in average clay minerals content as alumosity increases (Fig. 12B). However, these trends do not adequately convey the complexity of porcelain stoneware batch design: for example, the increase of clay minerals in peraluminous bodies is accompanied by a greater share of kaolinite. On the other hand, the decrease in fluxes with increasing alumosity is somewhat offset by the increase in the incidence of sodium feldspar on the total fluxes (Fig. 12B).

Vitrification paths have been investigated here for the first time over the whole compositional range of porcelain stoneware, but their definition still suffers from some limitations, mainly depending on important firing reactions that have not been sufficiently studied to allow their accurate prediction and modelling. These are, in particular, the efficiency of mullitisation and the degree of involvement of quartz in feldspar melting. Although mullite formation has been extensively investigated in the context of porcelain-like materials [2,8,13,20,52–55,60,61], it is not well understood how it varies upon different characteristics of kaolinite and illite, such as particle size and degree of structural disorder [62]. In addition, little is known about the stability of mullite in contact with the liquid phase at high temperature [30,63]. Melting of quartz and feldspar does not take place according to eutectics, but occurs with ratios that reflect a complex interplay between kinetics and thermodynamic equilibrium, where particle size and degree of alteration of raw materials can play a non-negligible role.

Meta-aluminous batches (MAL) can be obtained by compensating for the peraluminous character due to clay minerals through a significant substitution of feldspathic raw materials (10–20 wt%) with low alumina fluxes. This gives rise to highly polymerized, slightly peralkaline melts which, due to their lower viscosity and higher surface tension, ensure an early onset of densification and faster sintering rates compared to peraluminous batches. The peculiar vitrification path of the MAL bodies, which extensively involves quartz and mullite but favours the permanence/precipitation of feldspars, renders the typical buffering effect of porcelain stoneware largely ineffective, resulting in lower stability at high temperature and lower densification efficiency with respect to PAL batches.

Slightly peraluminous batches (PAL1) can be designed by using high amount of fluxes and selecting less aluminous clay materials (e.g., illite-kaolinite ball clay instead of kaolin) or even using small amounts of

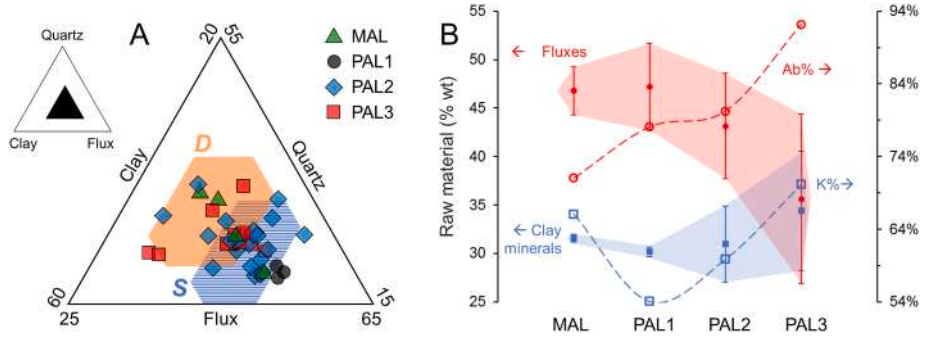

Fig. 12. A) Batch formulations of the four classes of porcelain stoneware in the Clay minerals-Fluxes-Quartz ternary diagram, compared with fields of white and super white bodies (S, after [1]) and batches with microstructure-oriented design (D, [21]). B) Amount of clay minerals and fluxes in the batches (mean value ± standard deviation) of the four classes of porcelain stoneware, with percentage of kaolinite over the sum of clay minerals (K%) and sodic feldspar over the sum of fluxes (Ab%).

low alumina fluxes (generally <5 %). These formulations produce metaaluminous to slightly peraluminous melts, which have higher viscosity than the liquid phases of the MAL batches and therefore higher densification start temperatures and slower sintering rates. However, the densification efficiency and stability at dwell temperature are on average better than those of the MAL bodies.

Frankly peraluminous batches (PAL2) have a flux-to-clay ratio intermediate between PAL1 and PAL3, stemming from the use of clay materials of average alumosity (ball clay prevalent on kaolin) together with silica sources and fluxes (in particular abundant sodic feldspar). The resulting liquid phases are moderately peraluminous in composition. PAL2 formulations allow maximum dimensional stability and good efficiency of densification to be achieved, despite the rather slow sintering kinetics and the slowest start of densification among porcelain stoneware batches.

Strongly peraluminous batches (PAL3) are characterized by the lowest flux-to-clay ratios and significant use of kaolin rather than ball clay. The resulting greater refractoriness is commonly compensated by the extensive use of sodium feldspar or strong fluxes (not the low-alumina ones). The liquid phases that form in these batches are the most peraluminous and least polymerized within the porcelain stoneware field, placing them at a certain distance from the liquidus surface at temperatures around 1200 °C. PAL3 formulations allow the maximum densification efficiency to be achieved, but on the other hand they have a slightly lower average dimensional stability at dwell temperature compared to PAL2 bodies.

4. Conclusions

The present study highlights the existence of different vitrification paths within the compositional perimeter of porcelain stoneware, which was investigated for the first time across its entire range on the basis of literature data and unpublished results for industrial and laboratory batches. Only bodies that fulfil the requirements for porcelain stoneware were considered: quantitative data of chemical-mineralogical composition of the batch, phase composition of fired body, and sintering behaviour were provided.

The phase transformations that give rise to the different vitrification paths – observed in previous studies for more or less narrow compositional ranges – were interpreted in relation to the SiO_2-Al_2O_3-Na_2O phase diagram. In this way it was possible to corroborate the observations of previous studies and to place them in a conceptual framework which allows the batch composition to be related to phase transformations during firing, liquid phase properties and sintering behaviour in a cause-and-effect manner. Thus, non-linear trends as a function of alumosity ($Al_2O_3/Al_2O_3+Na_2O + K_2O + CaO + MgO$) and silica content of batches emerge, consistent with the stability of the crystalline phases in contact with peralkaline or peraluminous melts, as predicted by the phase diagram.

Although the liquid phase forms in comparable amounts throughout the compositional range of porcelain stoneware, it is possible to identify chemical gradients suggesting a complex patchwork in which pseudo-structural parameters of the melts change mainly as a function of alumosity. These gradual variations have significant effects on the physical properties that govern the sintering behaviour, first of all the melt viscosity. The liquid phases in most of the porcelain stoneware range are more or less highly polymerized, with little variation in the values of pseudo-structural parameters. Nonetheless, there are important changes in the composition of glass network formers, modifiers, and charge compensators as a function of alumosity.

Crucial in this regard is the role of aluminium, as it can easily change its distribution between crystalline phases and melt, where it can simultaneously act as a glass network former and a modifier. Aluminium speciation is largely controlled by the formation and persistence of mullite, with a direct effect on the liquid phase. As the alumosity of porcelain stoneware batch increases, a greater quantity of mullite is formed (also thanks to a greater mullitisation index). The liquid phase reacts by increasing Al as glass network former (to the extent allowed by the availability of charge compensators) and then converting Al from former to modifier. These complex phenomena contribute to reducing the variation gradients of the melt viscosity, since Al as a glass network modifier has less impact than alkalis, and the viscosity-alumosity curve is much less steep on the peraluminous side than on the peralkaline side. Another relevant effect is the persistence/dissolution of quartz, which allows the loss of solid load (reduction in effective viscosity) to be compensated by increasing the silica content of the melt (increase in liquid phase viscosity). Therefore, there are two distinct mechanisms that spontaneously dampen variations in effective viscosity across the compositional range of porcelain stoneware.

Batch design has been revisited in relation to the chemical composition of the bodies, attempting for the first time to describe the dependence of performance on composition in terms of pros and cons. In this way, a predictive tool is available to complement the inescapable technological assessments in the formulation of porcelain stoneware batches.

CRediT authorship contribution statement

Sonia Conte: Writing – review & editing, Writing – original draft, Data curation, Conceptualization. **Chiara Molinari:** Writing – review & editing, Data curation. **Matteo Ardit:** Writing – review & editing, Data curation. **Daniele Giordano:** Writing – review & editing, Methodology. **Michele Dondi:** Writing – review & editing, Writing – original draft, Validation, Methodology, Investigation, Data curation, Conceptualization. **Chiara Zanelli:** Writing – review & editing, Supervision, Project administration.

Declaration of competing interest

The author Michele Dondi is an Editorial Board Member for this journal and was not involved in the editorial review or the decision to publish this article.

Acknowledgements

This work was funded by the Project ECOSISTER (ECS_00000033) under the National Recovery and Resilience Plan (NRRP), Mission 04 Component 2 Investment 1.5 – Next Generation EU.

Appendix A. Supplementary data

Supplementary data to this article can be found online at https://doi.org/10.1016/j.ceramint.2025.05.388.

References

[1] E. Sánchez, J. García-Ten, V. Sanz, A. Moreno, Porcelain tile: almost 30 years of steady scientific-technological evolution, Ceram. Int. 36 (3) (2010) 831–845.
[2] M. Romero, J.M. Pérez, Relation between the microstructure and technological properties of porcelain stoneware, A review. Materiales de Construcción 65 (2015) 65.
[3] J. García-Ten, M. Dondi, J. Vítor, M.V. Lisboa, M.V. Cabedo, L. Pérez-Villarejo, E. Rambaldi, C. Zanelli, Critical raw materials in the global high-throughput ceramic industry, Sustain. Mater. Technol. (2024) e00832.
[4] M. Dondi, M. Raimondo, C. Zanelli, Clays and bodies for ceramic tiles: reappraisal and technological classification, Appl. Clay Sci. 96 (2014) 91–109.
[5] L. Nodari, S. Conte, L. Casini, M. Sisti, R. Fantini, A.F. Gualtieri, C. Molinari, C. Zanelli, D. Giordano, M. Dondi, R. Arletti, Role of iron-rich clays on sintering of porcelain stoneware tiles, J. Eur. Ceram. Soc. 45 (2025) 116947.
[6] S. Conte, C. Molinari, S. Javed, M. Dondi, C. Zanelli, Compositional diversity of vitrified silicate ceramics: delimiting the chemical perimeter of industrial bodies, Ceram. Int. 22 (2024) 46157–46165.
[7] W.M. Carty, U. Senapati, Porcelain—Raw materials, processing, phase evolution, and mechanical behavior, J. Am. Ceram. Soc. 81 (1) (1998) 3–20.
[8] S. Conte, C. Molinari, M. Ardit, G. Cruciani, M. Dondi, C. Zanelli, Porcelain versus porcelain stoneware: so close, So different. Sintering kinetics, phase evolution, and vitrification paths, Materials 16 (1) (2023) 171.

[9] A.F. Gualtieri, Thermal behavior of the raw materials forming porcelain stoneware mixtures by combined optical and in situ x-ray dilatometry, J. Am. Ceram. Soc. 90 (4) (2007) 1222–1231.
[10] L. Carbajal, F. Rubio-Marcos, M.A. Bengochea, J.F. Fernandez, Properties related phase evolution in porcelain ceramics, J. Eur. Ceram. Soc. 27 (13–15) (2007) 4065–4069.
[11] Jr A. De Noni, D. Hotza, V.C. Soler, E.S. Vilches, Influence of composition on mechanical behaviour of porcelain tile. Part I: microstructural characterization and developed phases after firing, Mater. Sci. Eng., A 527 (7–8) (2010) 1730–1735.
[12] J. Martín-Márquez, A.G. De la Torre, M.A. Aranda, J.M. Rincón, M. Romero, Evolution with temperature of crystalline and amorphous phases in porcelain stoneware, J. Am. Ceram. Soc. 92 (1) (2009) 229–234.
[13] M. Lassinantti Gualtieri, M. Romagnoli, A.F. Gualtieri, Influence of body composition on the technological properties and mineralogy of stoneware: a DOE and mineralogical–microstructural study, J. Eur. Ceram. Soc. 31 (5) (2011) 673–685.
[14] L. Punsukumtana, S. Rugthaicharoencheep, W.T. Saengchantara, N. Suphanam, K. Sirinukunwattana, S. Pharaboon, Effect of firing temperatures on physical properties and phase evolutions of fine stoneware bodies, Key Eng. Mater. 608 (2014) 114–121.
[15] E.E. Gültekin, G. Topateş, S. Kurama, The effects of sintering temperature on phase and pore evolution in porcelain tiles, Ceram. Int. 43 (14) (2017) 11511–11515.
[16] S. Salem, A. Salem, Mechanisms of momentum transport in viscous flow sintering, Sinter. Appl. 1 (2013) 287–318.
[17] D. Giordano, Advances in the rheology of natural multiphase silicate melts: importance for magma transport and lava flow emplacement, Ann. Geophys. 61 (2019) 1–67.
[18] S. Conte, C. Zanelli, M. Ardit, G. Cruciani, M. Dondi, Phase evolution during reactive sintering by viscous flow: disclosing the inner workings in porcelain stoneware firing, J. Eur. Ceram. Soc. 40 (4) (2020) 1738–1752.
[19] C. Zanelli, M. Raimondo, G. Guarini, M. Dondi, The vitreous phase of porcelain stoneware: composition, evolution during sintering and physical properties, J. Non-Cryst. Solids 357 (16–17) (2011) 3251–3260.
[20] J.L. Amorós, E. Blasco, A. Moreno, C. Feliu, Kinetics of the transformations occurring during the firing process of an industrial spray-dried porcelain stoneware body, Ceram. Int. 48 (12) (2022) 17611–17620.
[21] Jr.A. De Noni, S.B. Canever, P. Henrique, R.R. da Silva, Microstructure-oriented porcelain stoneware tile composition design, Ceram. Int. 49 (14) (2023) 24558–24565.
[22] M. Zamani, H. Yapicioglu, A. Kara, C. Sevik, Statistical analysis of porcelain tiles' technical properties: full factorial design investigation on oxide ratios and temperature, Phys. Scripta 98 (2023) 125953.
[23] M. Dondi, G. Ercolani, C. Melandri, C. Mingazzini, M. Marsigli, The chemical composition of porcelain stoneware tiles and its influence on microstructural and mechanical properties, Interceram 48 (2) (1999) 75–83.
[24] E. Rambaldi, W.M. Carty, A. Tucci, L. Esposito, Using waste glass as a partial flux substitution and pyroplastic deformation of a porcelain stoneware tile body, Ceram. Int. 33 (5) (2007) 727–733.
[25] A. Salem, S.H. Jazayeri, E. Rastelli, G. Timellini, Dilatometeric study of shrinkage during sintering process for porcelain stoneware body in presence of nepheline syenite, J. Mater. Process. Technol. 209 (3) (2009) 1240–1246.
[26] N.T. Selli, Investigation of the whitening composition for the porcelain stoneware tiles, Acta Phys. Pol., A 127 (4) (2015) 1202–1204.
[27] J.L. Amorós, M.J. Orts, J. García-Ten, A. Gozalbo, E. Sánchez, Effect of the green porous texture on porcelain tile properties, J. Eur. Ceram. Soc. 27 (5) (2007) 2295–2301.
[28] J.M. Pérez, J.M. Rincón, M. Romero, Effect of moulding pressure on microstructure and technological properties of porcelain stoneware, Ceram. Int. 38 (1) (2012) 317–325.
[29] S. Salem, A. Salem, Shrinkage prediction during non-isothermal sintering in the presence liquid phase: new kinetic model, Part I, Thermochim. Acta 575 (2014) 322–330.
[30] V. Diella, I. Adamo, L. Pagliari, A. Pavese, F. Francescon, Effects of particle size distribution and starting phase composition in Na-feldspar/kaolinite system at high temperature, J. Eur. Ceram. Soc. 35 (4) (2015) 1327–1335.
[31] F. Contartesi, F.G. Melchiades, A.O. Boschi, Anticipated overfiring in porcelain tiles: effects of the firing cycle and green bulk density, Bol. Soc. Espanola Ceram. Vidr. 58 (2) (2019) 69–76.
[32] L.R. Dos Santos Conserva, F.G. Melchiades, S. Nastri, A.O. Boschi, M. Dondi, G. Guarini, M. Raimondo, C. Zanelli, Pyroplastic deformation of porcelain stoneware tiles: wet vs. dry processing, J. Eur. Ceram. Soc. 37 (2017) 333–342.
[33] C. Zanelli, R. Soldati, S. Conte, G. Guarini, A.I. Ismail, M.S. El-Maghraby, A. Cazzaniga, M. Dondi, Technological behavior of porcelain stoneware bodies with Egyptian syenites, Int. J. Appl. Ceram. Technol. 16 (2) (2019) 574–584.
[34] S. Conte, C. Zanelli, C. Molinari, G. Guarini, M. Dondi, Glassy wastes as feldspar substitutes in porcelain stoneware tiles: thermal behaviour and effect on sintering process, Mater. Chem. Phys. 256 (2020) 123613.
[35] S. Conte, D. Buonamico, T. Magni, R. Arletti, M. Dondi, G. Guarini, C. Zanelli, Recycling of bottom ash from biomass combustion in porcelain stoneware tiles: effects on technological properties, phase evolution and microstructure, J. Eur. Ceram. Soc. 42 (12) (2022) 5153–5163.
[36] C. Tavares Brasileiro, S. Conte, F. Contartesi, F.G. Melchiades, C. Zanelli, M. Dondi, A.O. Boschi, Effect of strong mineral fluxes on sintering of porcelain stoneware tiles, J. Eur. Ceram. Soc. 41 (11) (2021) 5755–5767.
[37] C. Tavares Brasileiro, H.D. de Almeida Filho, G.L. Santana, A.V. Lot, S. Conte, C. Zanelli, M. Dondi, O.A. Boschi, Sericite instead of feldspar in porcelain stoneware: effect on sintering and phase evolution, Int. J. Appl. Ceram. Technol. 19 (1) (2022) 612–622.
[38] C. Molinari, Y. Alaya, L. Pasti, G. Guarini, M. Dondi, C. Zanelli, Assessing white clays from Tabarka (Tunisia) in the production of porcelain stoneware tiles, Appl. Clay Sci. 231 (2023) 106741.
[39] S. Conte, R. Fantini, R. Arletti, C. Molinari, M. Dondi, C. Zanelli, A.F. Gualtieri, Sintering mechanisms, phase transformations and microstructure of porcelain stoneware containing thermally inertized man-made vitreous fibres, J. Eur. Ceram. Soc. 45 (2025) 117230.
[40] C. Zanelli, G. Baldi, M. Dondi, G. Ercolani, G. Guarini, M. Raimondo, Glass–ceramic frits for porcelain stoneware bodies: effects on sintering, phase composition and technological properties, Ceram. Int. 34 (3) (2008) 455–465.
[41] V. Cannillo, L. Esposito, E. Rambaldi, A. Sola, A. Tucci, Effect of porosity on the elastic properties of porcelainized stoneware tiles by a multi-layered model, Ceram. Int. 35 (1) (2009) 205–211.
[42] M. Raimondo, C. Zanelli, G. Guarini, M. Dondi, R. Fabbroni, T. Cortesi, Process of pyroplastic shaping for special-purpose porcelain stoneware tiles, Ceram. Int. 35 (5) (2009) 1975–1984.
[43] N.T. Selli, Development of anorthite based white porcelain stoneware tile compositions, Ceram. Int. 41 (6) (2015) 7790–7795.
[44] M.L. Ligabue, A.F. Gualtieri, M. Lassinantti Gualtieri, D. Malferrari, G. Lusvardi, Recycling of thermally treated cement-asbestos for the production of porcelain stoneware slabs, J. Clean. Prod. 247 (2020) 119084.
[45] S. Conte, C. Zanelli, M. Ardit, G. Cruciani, M. Dondi, Predicting viscosity and surface tension at high temperature of porcelain stoneware bodies: a methodological approach, Materials 11 (12) (2018) 2475.
[46] T. Ban, K. Okada, Structure refinement of mullite by the Rietveld method and a new method for estimation of chemical composition, J. Am. Ceram. Soc. 75 (1) (1992) 227–230.
[47] G.S. Prata, L.J. Ventress, E. Carboni, T.A. Mather, R.G. Grainger, D.M. Pyle, A new parameterization of volcanic ash complex refractive index based on NBO/T and SiO2 content, J. Geophys. Res. Atmos. 124 (3) (2019) 1779–1797.
[48] B. Mysen, P. Richet, Silicate Glasses and Melts, Elsevier, 2018.
[49] D. Giordano, J.K. Russell, D.B. Dingwell, Viscosity of magmatic liquids: a model, Earth Planet Sci. Lett. 271 (1–4) (2008) 123–134.
[50] A. Costa, L. Caricchi, N. Bagdassarov, A model for the rheology of particle-bearing suspensions and partially molten rocks, Geochem. Geophys. Geosystems 10 (3) (2009) Q03010.
[51] J. Vasseur, F.B. Wadsworth, Y. Lavallée, K.U. Hess, D.B. Dingwell, Volcanic sintering: timescales of viscous densification and strength recovery, Geophys. Res. Lett. 40 (21) (2013) 5658–5664.
[52] G.P. Souza, E. Rambaldi, A. Tucci, L. Esposito, W.E. Lee, Microstructural variation in porcelain stoneware as a function of flux system, J. Am. Ceram. Soc. 87 (10) (2004) 1959–1966.
[53] M. Romero, J. Martín-Márquez, J.M. Rincón, Kinetic of mullite formation from a porcelain stoneware body for tiles production, J. Eur. Ceram. Soc. 26 (9) (2006) 1647–1652.
[54] J.M. Pérez, J.M. Rincón, M. Romero, Study of mullite formation in porcelain stoneware applying isoconversional and IKP methods, Ceram. Int. 36 (8) (2010) 2329–2335.
[55] D. Magagnin, C.M.F. dos Santos, A. Wanderlind, J. Jiusti Jr., A. De Noni Effect of kaolinite, illite and talc on the processing properties and mullite content of porcelain stoneware tiles, Mater. Sci. Eng., A 618 (2014) 533–539.
[56] A. Tucci, E. Rambaldi, L. Esposito, Use of scrap glass as raw material for porcelain stoneware tiles, Adv. Appl. Ceram. 105 (1) (2006) 40–45.
[57] A. Tucci, L. Esposito, L. Malmusi, E. Rambaldi, New body mixes for porcelain stoneware tiles with improved mechanical characteristics, J. Eur. Ceram. Soc. 27 (2–3) (2007) 1875–1881.
[58] A.F. Gualtieri, Development of low-firing b-fluxed stoneware tiles, J. Am. Ceram. Soc. 92 (11) (2009) 2571–2577.
[59] E. Rambaldi, L. Esposito, F. Andreola, L. Barbieri, I. Lancellotti, I. Vassura, The recycling of MSWI bottom ash in silicate based ceramic, Ceram. Int. 36 (8) (2010) 2469–2476.
[60] W.E. Lee, Y. Iqbal, Influence of mixing on mullite formation in porcelain, J. Eur. Ceram. Soc. 21 (14) (2001) 2583–2586.
[61] W.E. Lee, G.P. Souza, C.J. McConville, T. Tarvornpanich, Y. Iqbal, Mullite formation in clays and clay-derived vitreous ceramics, J. Eur. Ceram. Soc. 28 (2) (2008) 465–471.
[62] I. Adamo, V. Diella, A. Pavese, P. Vignola, F. Francescon, Na-feldspar (F) and kaolinite (K) system at high temperature: resulting phase composition, micro-structural features and mullite-glass Gibbs energy of formation, as a function of F/K ratio and kaolinite crystallinity, J. Eur. Ceram. Soc. 33 (15–16) (2013) 3387–3395.
[63] N. Marinoni, D. D'Alessio, V. Diella, A. Pavese, F. Francescon, Effects of soda–lime–silica waste glass on mullite formation kinetics and micro-structures development in vitreous ceramics, J. Environ. Manag. 124 (2013) 100–107.
[64] C. Molinari, S. Conte, M. Dondi, C. Zanelli, Content of crystalline silica phases in porcelain stoneware, Open Ceram. 19 (2024) 100650.
[65] M.J. Jackson, B. Mills, Dissolution of quartz in vitrified ceramic materials, J. Mater. Sci. 32 (1997) 5295–5304.
[66] F. Matteucci, M. Dondi, G. Guarini, Effect of soda-lime glass on sintering and technological properties of porcelain stoneware tiles, Ceram. Int. 28 (8) (2002) 873–880.
[67] E. Bernardo, L. Esposito, E. Rambaldi, A. Tucci, S. Hreglich, Recycle of waste glass into "glass–ceramic stoneware", J. Am. Ceram. Soc. 91 (7) (2008) 2156–2162.

[68] E. Bernardo, L. Esposito, E. Rambaldi, A. Tucci, Glass based stoneware'as a promising route for the recycling of waste glasses, Adv. Appl. Ceram. 108 (1) (2009) 2–8.
[69] M. Lassinantti Gualtieri, C. Mugoni, S. Guandalini, A. Cattini, D. Mazzini, C. Alboni, C. Siligardi, Glass recycling in the production of low-temperature stoneware tiles, J. Clean. Prod. 197 (2018) 1531–1539.
[70] M.M. Raith, R. Hoffbauer, B. Spiering, M. Shinoto, N. Nakamura, Melting behaviour of feldspar clasts in high-fired Sue ware, Eur. J. Mineral 28 (2) (2016) 385–407.
[71] E. Bernardo, L. Esposito, S. Hreglich, E. Rambaldi, G. Timellini, A. Tucci, Tailored waste based glasses as secondary raw materials for porcelain stoneware, Adv. Appl. Ceram. 107 (6) (2008) 322–328.
[72] S.Y.R. Lopez, J.S. Rodriguez, S.S. Sueyoshi, Determination of the activation energy for densification of porcelain stoneware, J. Ceram. Process. Res. 12 (3) (2011) 228–232.
[73] R.G. Kuryaeva, Degree of polymerization of aluminosilicate glasses and melts, Glass Phys. Chem. 30 (2004) 157–166.
[74] W.M. Carty, Observations on the glass phase composition in porcelains, Mater. Equip. Whitewares: Ceram. Eng. Sci. Proc. 23 (2002) 79–94.
[75] I.A. Pavlova, A.S. Kiyko, E.P. Farafontova, Effect of chemical composition of glassy phase of porcelain stoneware on product brittleness, Mater. Sci. Forum 989 (2020) 254–259.
[76] H. Lee, W. Carty, The glass formation boundary in aluminosilicates, Int. J. Appl. Glass Sci. 13 (4) (2022) 708–719.
[77] J.V. Owen, J. Dostal, Phase-equilibrium constraints on kiln temperatures at the Eby pottery (ca. 1857–1905), Conestogo, Ontario, Can. Mineral. 44 (5) (2006) 1257–1266.
[78] A. Tsuchiyama, E. Takahashi, Melting kinetics of a plagioclase feldspar, Contrib. Mineral. Petrol. 84 (1983) 345–354.
[79] M.J. Toplis, D.B. Dingwell, T. Lenci, Peraluminous viscosity maxima in Na2O-Al2O3-SiO2 liquids: the role of triclusters in tectosilicate melts, Geochem. Cosmochim. Acta 61 (13) (1997) 2605–2612.
[80] C. Le Losq, D.R. Neuville, P. Florian, G.S. Henderson, D. Massiot, The role of Al^{3+} on rheology and structural changes in sodium silicate and aluminosilicate glasses and melts, Geochem. Cosmochim. Acta 126 (2014) 495–517.
[81] E.F. Riebling, Structure of sodium aluminosilicate melts containing at least 50 mole % SiO_2 at 1500° C, J. Chem. Phys. 44 (8) (1966) 2857–2865.
[82] K. Hunold, R. Brückner, Physikalische Eigenschaften und struktureller Feinbau von Natrium-Aluminosilicatgllsem und -schmelzen, Glastech. Ber. 6S (1980) 149–161.
[83] S.L. Webb, E. Müller, H. Büttner, Anomalous rheology of peraluminous melts, Am. Mineral. 89 (5–6) (2004) 812–818.
[84] D. Giordano, A. Mangiacapra, M. Potuzak, J.K. Russell, C. Romano, D.B. Dingwell, A. Di Muro, An expanded Non-Arrhenian model for silicate melt viscosity: a treatment for metaluminous, peraluminous and peralkaline liquids, Chem. Geol. 229 (1–3) (2006) 42–56.
[85] J. Pinter Junior, A. Zaccaron, S. Arcaro, J.B.R. Neto, A. de Noni Junior, F. R. Pereira, Novel approach to ensure the dimensional stability of large-format enameled porcelain stoneware tiles through water absorption control, Open Ceram. 9 (2022) 100203.
[86] F.B. Wadsworth, J. Vasseur, E.W. Llewellin, J. Schauroth, K.J. Dobson, B. Scheu, D. B. Dingwell, Sintering of viscous droplets under surface tension, Proc. R. Soc. A 472 (2188) (2016) 20150780.
[87] F.B. Wadsworth, J. Vasseur, E.W. Llewellin, D.B. Dingwell, Hot sintering of melts, glasses and magmas, Rev. Mineral. Geochem. 87 (1) (2022) 801–840.
[88] A.M. Buchtel, W.M. Carty, M.D. Noirot, Pyroplastic deformation revisited, Whitewares Mater.: Ceram. Eng. Sci. Proc. 25 (2004) 25–42.
[89] E. Sánchez, V. Sanz, E. Cañas, J. Sales, K. Kayacı, M.U. Taşkıran, Ş. Türk, Revisiting pyroplastic deformation. Application for porcelain stoneware tile bodies, J. Eur. Ceram. Soc. 39 (2–3) (2019) 601–609.

SUPPLEMETARY MATERIALS

Table S1 (supplementary material)
Chemical composition (dry basis) and mineralogical composition of unfired batches. Phase composition of fired porcelain stoneware bodies.

	[34]							[36]				[8]			[40]				[37]	
% weight	**I0**	**B2**	**F2**	**L2**	**S2**	**G2**	**G4**	**STD**	**W6.5**	**D12**	**P14**	**GSTO**	**GPOR**	**POST**	**BR**	**BF0**	**BF1**	**BF5**	**ser-S**	**ser-F**
SiO_2	70.81	70.61	68.21	70.73	68.75	70.66	70.52	71.36	69.74	69.47	68.43	72.53	71.66	71.97	73.81	71.14	71.59	71.65	76.76	73.76
TiO_2	0.70	0.66	0.66	0.65	0.72	0.79	0.87	0.98	0.92	0.87	0.89	0.61	0.50	0.78	0.54	0.48	0.48	0.48	0.79	0.02
Al_2O_3	19.93	17.17	18.76	16.88	17.09	20.24	20.55	18.51	17.33	16.66	18.84	16.53	19.35	20.02	17.47	17.68	15.67	16.84	16.76	15.01
Fe_2O_3	0.74	0.72	0.68	0.67	0.66	0.89	1.04	2.19	2.07	2.01	2.40	0.58	0.42	0.51	0.58	0.52	0.52	0.52	1.01	0.18
MgO	0.44	0.78	0.60	0.95	0.42	0.46	0.48	2.34	2.25	4.16	2.17	1.07	0.70	0.66	0.49	1.39	0.43	1.17	1.04	0.00
CaO	0.86	2.58	2.66	1.59	0.82	0.92	0.98	0.17	3.13	2.63	0.36	2.50	0.43	0.59	0.58	2.94	3.75	2.27	0.03	0.19
Na_2O	3.64	5.05	3.14	5.89	4.02	3.13	2.62			0.06	1.46	5.03	6.13	4.40	4.16	3.72	3.72	3.72	0.19	2.99
K_2O	2.87	2.43	2.84	2.47	3.69	2.78	2.70	3.32	3.11	3.04	3.46	1.16	0.81	1.07	2.27	2.03	2.03	2.29	3.42	7.84
ZrO_2				0.01	0.39	0.09	0.19	0.24	0.22	0.21	0.22				0.00	0.00	1.69	0.96		
others			2.45	0.14	3.43															
Alumosity*	73.56	61.62	64.00	60.99	63.77	75.11	76.67	75.61	65.90	59.45	71.60	62.94	73.90	74.71	71.29	62.85	61.35	63.86	66.25	66.05
Illite +I/S	11	11	11	11	11	11	10	8	8	7	9	13	10	13					37	16
Kaolinite	22	21	21	21	21	21	20	20	26	25	25	19	19	20					18	26
Quartz	23	19	19	19	19	24	24	32	31	30	31	24	25	28					38	40
Plagioclase	27	18	18	18	18	18	10	1	1	1	14	22	44	37					1	5
K-feldspar	15	10	10	10	10	10	5	31	20	20	18	<1	1	<1					2	8
Glass		20	20	20	20	13	26					20								
Fe-oxides	1	1	1	1	1	1	<1	2	2	2	2	<1	<1	1					2	1
Accessories	1	1	1	1	1	2	4	8	14	17	1	1	1	1					4	3
Quartz	23.2	14.0	16.0	15.9	13.3	23.0	22.4	27.2	25.8	28.9	24.4	14.9	20.1	20.4	20.5	18.0	13.7	17.9	20.0	28.2
Mullite	5.9	1.9	3.4	0.5	1.3	7.4	9.3	7.7	3.9	3.7	3.6	4.6	6.9	3.0	5.7	4.7	3.5	4.8	6.9	6.8
Plagioclase	4.7	10.4	9.3	11.3	3.0	2.2	0.8	0.5	3.3	1.8	0.9	19.1	6.4	3.5	5.3	15.7	11.8	11.7	0.5	1.9
K-Feldspar	4.6	3.2	10.6	2.2	12.1	0.4	0.3		1.4	1.0		1.6	1.0	1.9	1.2	3.4	2.5	2.2		
Zircon																			0.7	0.8
Vitreous phase	61.6	70.5	60.7	70.1	70.3	67.0	67.2	64.6	65.6	62.1	71.1	59.7	65.6	71.2	67.3	58.2	66.1	62.9	71.9	62.3

*$[Al_2O_3/(Al_2O_3+Na_2Oeq)*100]$

Table S1 (continued)

Chemical composition (dry basis) and mineralogical composition of unfired batches. Phase composition of fired porcelain stoneware bodies.

	[39]		[33]				[35]		[18]						[32]		
% weight	**V0**	**V6**	**EG0**	**EAS3**	**ENS3**	**EQS3**	**C0**	**C6**	**NA**	**NAB**	**AT**	**ATP**	**NAK**	**K**	**W7**	**W12**	**W9**
SiO_2	70.90	69.23	70.41	68.87	68.73	67.93	72.04	70.53	70.00	71.04	72.73	73.89	69.66	69.31	69.55	67.79	67.56
TiO_2	0.65	0.70	0.72	0.63	0.63	0.61	0.62	0.64	0.72	0.22	0.60	0.54	0.67	0.63	0.24	0.24	0.26
Al_2O_3	20.79	20.51	20.20	20.78	20.84	21.25	19.48	18.97	21.27	20.98	18.76	17.50	20.96	20.65	21.38	22.85	23.34
Fe_2O_3	0.46	0.98	0.72	0.80	0.78	0.76	0.56	0.82	0.46	0.56	0.62	0.58	0.45	0.44	0.43	0.46	0.47
MgO	0.59	1.26	0.72	0.69	0.69	0.69	0.36	0.61	0.30	0.41	0.24	0.49	0.28	0.27	1.31	1.30	1.30
CaO	0.55	1.75	0.80	0.65	0.65	0.61	0.45	2.12	0.38	0.77	0.79	0.58	0.34	0.30	0.82	0.71	0.71
Na_2O	4.73	4.22	3.82	3.39	3.55	3.87	4.16	3.87	5.66	4.76	4.51	4.16	3.67	1.69	3.44	2.98	2.94
K_2O	1.32	1.34	2.62	4.21	4.15	4.27	2.32	2.44	1.21	1.25	1.74	2.27	3.96	6.71	0.67	1.51	1.25
ZrO_2															2.12	2.13	2.13
others																	
Alumosity*	74.46	69.55	72.84	72.38	72.13	71.63	74.28	70.30	74.35	74.81	73.12	71.29	74.75	75.09	75.88	77.20	78.08
Illite +I/S	12	12	17	17	17	17	18	25	4	4	5	6	5	16	8	14	12
Kaolinite	21	20	15	14	14	14	11	11	23	23	18	16	23	16	32	32	36
Quartz	22	22	23	19	20	19	26	26	19	23	27	29	19	20	27	24	25
Plagioclase	40	34	33	35	36	35	40	30	48	42	41	37	32	15	29	24	25
K-feldspar	3	3	10	15	14	14	5	4	6	5	8	11	20	31	1	3	3
Glass		6						6						1			
Fe-oxides	<1	1	1	1	1	1	<1	<1	<1	1	1	1	<1	1		<1	<1
Accessories	2	2	1			1			1	1	1	1	1	1	4	4	
Quartz	21.9	18.8	19.7	17.7	20.2	19.2	21.4	21.5	17.8	19.1	23.5	22.0	19.7	18.6	17.4	15.5	13.8
Mullite	9.9	7.8	10.2	9.7	9.9	9.0	9.5	6.8	10.2	9.6	7.0	6.1	9.9	9.9	11.5	12.6	14.0
Plagioclase	5.0	9.4	3.0		1.5	2.8	1.5	20.2	8.3	2.4	2.0			1.6	1.1		
K-Feldspar				2.8	3.9		1.7	3.7									
Zircon																	
Vitreous phase	63.2	64.0	67.1	69.8	64.5	68.9	65.8	47.7	63.8	69.0	67.3	71.6	70.5	69.9	67.7	69.6	69.9

*$[Al_2O_3/(Al_2O_3+Na_2Oeq)*100]$

Table S1 (continued)

Chemical composition (dry basis) and mineralogical composition of unfired batches. Phase composition of fired porcelain stoneware bodies.

	[42]									[38]			[44]	[15]	[41]	[26]	
% weight	**CE**	**CO**	**IN**	**KD**	**KO**	**KT**	**LI**	**OS**	**RU**	**TaB**	**TaC**	**TaD**	**L20**	**G17**	**C17**	**S15a**	**S15c**
SiO_2	73.70	73.96	74.31	72.96	69.47	69.75	74.71	69.79	69.36	70.15	70.44	68.81	67.68	75.17	70.13	73.54	71.01
TiO_2	0.43	0.45	0.42	0.33	0.46	0.55	0.67	0.56	0.72	0.96	0.69	0.65	0.53	0.58	0.94	0.45	0.23
Al_2O_3	16.25	16.23	15.84	16.42	18.04	17.88	16.13	19.21	19.35	21.55	20.54	21.56	23.96	17.83	19.55	16.49	20.14
Fe_2O_3	0.73	0.79	0.72	0.90	1.11	0.52	0.77	0.66	0.63	0.53	0.64	1.25	0.52	0.33	0.44	0.66	0.64
MgO	0.44	0.45	0.50	0.42	0.30	0.40	0.50	0.72	0.75	0.21	0.46	0.56	0.59	0.29	0.58	1.00	0.69
CaO	1.62	1.56	1.60	1.38	1.27	1.29	1.64	1.89	1.93	0.74	0.74	0.79	0.63	0.37	0.73	1.47	2.44
Na_2O	2.95	4.02	4.04	4.42	4.88	4.93	3.07	5.36	5.55	4.85	4.80	4.81	3.92	3.42	5.20	3.17	4.32
K_2O	2.37	2.40	2.42	1.55	1.55	1.57	2.38	1.62	1.47	1.01	1.69	1.57	1.90	1.81	2.43	0.53	0.53
ZrO_2	1.52	0.14	0.15	1.61	2.93	3.11	0.14	0.19	0.24							2.69	
others																	
Alumosity*	69.96	66.94	65.97	68.33	69.91	69.08	69.09	66.63	66.37	76.40	73.43	74.00	77.96	76.53	69.70	71.16	72.57
Illite +I/S										10	15	9					
Kaolinite										21	16	24					
Quartz										21	21	19					
Plagioclase										41	42	41					
K-feldspar										6	5	6					
Glass																	
Fe-oxides										<1	<1	1					
Accessories										1	1	1					
Quartz	28.8	24.5	26.5	21.7	18.0	16.3	27.3	15.1	14.3	11.2	10.3	9.9	17.2	35.7	24.2	28.0	19.0
Mullite	6.5	5.9	5.1	5.7	6.0	5.5	5.9	6.1	4.8	12.1	11.1	10.1	11.8	5.7	4.2	6.3	10.1
Plagioclase		6.7	6.3	1.2	6.8	8.8	1.4	20.0	22.1	1.9	5.2	3.0	1.9	1.6			10.6
K-Feldspar	3.8	2.0	4.0	2.4	2.5	2.4	2.7	6.5	4.6				1.0				
Zircon																	
Vitreous phase	59.2	60.9	58.1	67.2	62.1	63.0	62.7	52.3	54.2	74.8	73.4	77.0	68.2	57.0	71.6	61.7	60.5

*$[Al_2O_3/(Al_2O_3+Na_2Oeq)*100]$

Table S1 (continued)

Chemical composition (dry basis) and mineralogical composition of unfired batches. Phase composition of fired porcelain stoneware bodies.

	unpublished												
% weight	**C**	**E**	**V0**	**GF5**	**GF9**	**GR**	**G1**	**G2**	**GPO**	**AM**	**FW**	**P2**	**P4**
SiO_2	68.89	68.24	70.75	67.68	65.72	67.92	69.92	69.67	70.85	71.90	65.92	70.41	70.00
TiO_2	0.38	0.31	0.73	0.67	0.60	0.79	0.93	0.80	0.56	0.67	0.37	0.78	0.85
Al_2O_3	19.00	19.23	21.46	20.64	21.46	22.02	21.02	20.71	21.45	18.72	23.76	20.58	21.22
Fe_2O_3	1.11	1.01	0.45	2.93	3.06	1.20	0.80	1.49	0.43	0.62	0.34	0.95	1.15
MgO	0.42	0.32	0.09	1.35	1.33	0.75	0.73	0.75	0.55	0.24	0.21	0.44	0.44
CaO	0.67	0.42	0.27	1.06	1.22	0.98	1.13	1.67	0.40	0.92	0.79	0.86	0.86
Na_2O	2.49	3.36	4.78	3.83	3.94	2.95	3.01	2.96	4.74	5.08	4.89	3.21	2.77
K_2O	2.52	2.99	1.47	1.81	2.65	3.28	2.41	1.81	1.02	1.84	1.19	2.66	2.46
ZrO_2	4.56	4.40		0.03	0.02	0.10	0.04	0.13			2.53	0.07	0.14
others													
Alumosity*	77.44	75.37	77.61	71.41	70.27	74.95	75.08	74.32	76.20	70.92	77.57	75.66	77.75
Illite +I/S				17	17	21	13	9	8	10	5	11	10
Kaolinite				19	18	21	22	23	27	14	28	21	20
Quartz				22	19	24	25	27	23	25	16	23	22
Plagioclase				34	36	24	30	32	38	43	42	18	10
K-feldspar				6	8	7	9	8	3	8	5	10	5
Glass												14	28
Fe-oxides				2	2	1	1	1		1	<1	1	<1
Accessories				1	1	3			1		4	2	3
Quartz	24.9	21.4	18.5	23.1	17.1	23.9	24.8	25.5	13.6	24.0	15.7	23.3	20.5
Mullite	14.4	13.4	9.0	7.5	4.3	7.4	4.8	6.9	8.8	5.2	7.4	9.9	11.5
Plagioclase	0.7	0.4	3.2	3.9	1.0	3.8	2.0	1.8	10.0	5.4	3.4	1.3	0.5
K-Feldspar	0.4		1.2	1.1	1.5	3.9			1.5	1.3		0.5	0.2
Zircon											2.4		
Vitreous phase	52.1	57.4	68.2	64.4	76.1	60.9	68.3	65.8	66.1	64.1	71.1	65.0	67.3

*$[Al_2O_3/(Al_2O_3+Na_2Oeq)*100]$

Table S2 (supplementary material)
Methods followed for calculation of parameters used in data interpretation.

Parameter	Definition
Alumosity	Ratio of alumina to the sum of alumina and total flux oxides (wt%): $Al_2O_3/(Al_2O_3+Na_2O_{eq})*100$. Contribution of K, Ca and Mg are included in the Na_2O_{eq} parameter, calculated as the sum $Na_2O + MgO + CaO + K_2O$, having care to express the data as Na_2O equivalents using the following molar ratios: 1.538 (MgO), 1.105 (CaO), 0.658 (K_2O).
Chemical composition of mullite	Formula $Al_{4+2x}Si_{2-2x}O_{10-x}$ (0.17<x<0.59) $Al_2O_3^{MU}$ (mol%) = (1443**a*) – 1028.06; $SiO_2^{MU} = 100 - Al_2O_3^{MU}$, where *a* = length of *a* axis of the unit cell of mullite (nm)
Mullitisation index	Ratio between mullite in the ceramic body and mullite potentially formed by kaolinite and illite in the batch: Mullite/(potential Mullite) where potential Mullite = (f_k * %wt kaolinite) + (f_i * %wt illite); factors $f_k = 0.55$ and $f_i = 0.30$ by stoichiometry of firing reactions: $1.125 \cdot Al_4Si_4O_{10}(OH)_8$ (kaolinite) = $Al_{4.5}Si_{1.5}O_{9.75}$ (mullite) + $3 \cdot SiO_2$ (amorphous silica) + $4.5 \cdot H_2O$ (water vapour) $1.8 \cdot (K_{0.56},H_3O_{0.44})Mg_{0.4}Al_{2.2}Si_{3.5}O_{10}(OH)_2$ (illite) = $0.66 \cdot Al_{4.5}Si_{1.5}O_{9.75} + 1.0 \cdot KAlSi_3O_8 + 0.7 \cdot MgO + 2.1 \cdot SiO_2 + 2.2 \cdot H_2O$
Quartz variation (%)	$100 * (Q_{b'} – Q_c) / Q_{b'}$, where Q_c is the amount of quartz in the ceramic body and $Q_{b'}$ is the amount of quartz in the batch, normalized to the loss of ignition: $Q_{b'} = 100 * Q_b / (100 – L.o.I.)$
Feldspars variation (%)	$100 * (F_{b'} – F_c) / F_{b'}$, where F_c is the amount of feldspar in the ceramic body and $F_{b'}$ is the amount of feldspar in the batch, normalized to the loss of ignition: $F_{b'} = 100 * F_b / (100 – L.o.I.)$; F can be either plagioclase or K-feldspar, or their sum.
Quartz/feldspars melted fractions ratio	Ratio between the quartz variation and the feldspars variation after firing: $(Q_{b'} – Q_c) / (F_{b'} – F_c)$ It represents the fraction of quartz melted every unity fraction of feldspars melted.
Degree of polymerization of the melt (NBO/T)	From the composition of the liquid phase: Number of Non-Bridging Oxygens (NBO) per Tetrahedrally-coordinated cations (Si, Al) as atomic percentage.
Charge compensated aluminium in tetrahedral coordination (CCAT)	From the composition of the liquid phase: Al^{3+} charge compensated by alkali and alkaline earths: CCAT (atom%) = Na + K + 2Ca + 2Mg (up to max value = Al)
Alumina excess in the melt (Al_{ex})	Alumina in the liquid phase exceeding the CCAT, corresponding to Al^{3+} with oxygen coordination higher than 4: Al_{ex} (atom%) = Al (total) – CCAT
Glass network formers (GNF)	From the composition of the liquid phase: GNF (atom%) = Si + CCAT, corresponding to Al^{3+} charge compensated by alkali or alkaline earths
Glass network modifiers (GNM)	From the composition of the liquid phase: alkali and alkaline earths exceeding CCAT: GNM (atom%) = Na + K + Mg + Ca – CCAT
STAF	Empirical parameter, defined as the sum of $SiO_2 + a TiO_2 + b Al_2O_3 + c FeO_{tot}$, in molar percentage, where *a*, *b* and *c* are adjustable parameters.
Relative viscosity (η_{rel})	estimated from the steric effect of crystals dispersed in the liquid phase by the Costa's relation: $\eta_{rel} = [1-(\phi/\phi m)]^{-B\phi m}$, where ϕ is the solid load, ϕ_m is the critical fraction (set to 0.72) – below which the relative viscosity starts to lower – and *B* is the Einstein constant (*i.e., B* =2.5)
Effective viscosity (η_{eff})	the effective viscosity of the body (η_{eff}, Pa·s) is the product of the viscosity of the liquid phase (η_{melt}, Pa·s) by the relative viscosity (h_{rel}, adim.): $\eta_{eff} = \eta_{rel} \cdot \eta_{melt}$.

Table S3 (supplementary material)

Chemical composition, pseudo-structural parameters, and physical properties of the liquid phase. Sintering behaviour of porcelain stoneware.

		[34]							[36]				[8]			[40]				[37]	
property	**unit**	**I0**	**B2**	**F2**	**L2**	**S2**	**G2**	**G4**	**STD**	**W6.5**	**D12**	**P14**	**GSTO**	**GPOR**	**POST**	**BR**	**BF0**	**BF1**	**BF5**	**ser-S**	**ser-F**
Firing temperature	°C	1200	1200	1200	1160	1220	1200	1220	1215	1185	1185	1170	1200	1200	1225	1220	1220	1240	1220	1225	1195
SiO_2	%wt	65.77	67.24	63.42	65.76	64.49	65.56	66.66	66.02	63.23	60.28	61.46	66.30	68.40	68.51	70.38	66.83	69.64	68.44	71.04	68.37
TiO_2	%wt	0.99	0.93	1.10	0.94	1.59	1.32	1.58	1.90	1.76	1.75	1.59	1.02	0.76	1.05	0.80	0.83	0.76	0.76	1.17	0.85
Al_2O_3	%wt	21.39	18.19	20.14	19.27	18.84	21.41	20.28	19.63	20.02	21.21	22.83	19.76	19.34	23.23	18.05	18.27	15.86	17.08	15.32	17.46
FeOtot	%wt	1.04	1.03	1.12	0.97	0.94	1.33	1.54	3.42	3.19	3.26	3.43	0.97	0.64	0.77	0.86	0.89	0.79	0.83	2.04	1.69
MgO	%wt	0.63	1.10	0.99	1.36	0.61	0.70	0.73	3.65	3.47	6.01	3.10	1.78	1.07	1.13	0.72	2.39	0.67	1.86	3.94	4.58
CaO	%wt	1.17	3.04	3.73	1.59	0.99	1.25	1.43	0.11	3.81	2.64	0.46	3.85	0.55	0.63	0.86	5.06	4.90	3.61	2.31	2.59
Na_2O	%wt	5.03	5.79	3.75	6.90	5.32	4.37	3.79	0.00	0.00	0.10	1.97	4.84	8.25	3.61	5.26	3.22	3.56	3.74	0.23	0.74
K_2O	%wt	3.99	2.68	1.73	3.00	2.34	4.05	3.94	5.18	4.44	4.66	4.95	1.48	0.98	1.08	3.07	2.51	2.45	3.05	3.94	3.73
others	%wt			4.04	0.21	4.89															
Alumosity*	%wt	68.35	59.05	60.22	60.07	62.51	69.30	69.06	68.21	61.62	58.06	68.48	61.40	63.45	77.50	65.90	56.38	57.73	57.53	57.25	57.16
Solid load	1	0.384	0.295	0.393	0.299	0.297	0.330	0.328	0.354	0.344	0.379	0.289	0.403	0.344	0.288	0.327	0.418	0.339	0.371	0.281	0.377
NBOT	at	0.236	0.058	0.050	0.047	0.033	0.298	0.259	0.275	0.083	0.134	0.324	0.040	0.054	0.541	0.127	0.087	0.062	0.068	0.09	0.09
GNF	%at	39.0	40.8	40.3	40.5	40.1	37.3	38.8	39.8	41.5	42.0	40.1	41.5	41.0	38.3	40.40	40.77	40.95	41.00	40.2	40.2
Al fra GNF	%	21%	23%	26%	24%	25%	21%	20%	18%	22%	25%	21%	22%	20%	19%	19%	23%	20%	22%	20%	23%
GNM	%at	3.67	1.68	3.35	1.51	3.30	5.53	3.63	1.53	1.36	1.87	2.12	1.01	1.23	5.14	2.58	2.67	2.04	1.88	1.47	1.58
Al fra GNM	%	84%	16%	0%	29%	0%	78%	86%	77%	0%	0%	80%	0%	100%	100%	80%	5%	0%	1%	0%	0%
CCAT	%at	8.25	9.36	10.66	9.76	9.97	7.86	7.60	10.60	10.60	11.23	9.99	10.46	9.01	7.28	7.50	9.53	8.39	9.01	8.30	9.60
NaK fra CCAT	%	85%	70%	40%	78%	59%	69%	80%	65%	43%	42%	72%	46%	77%	69%	86%	47%	56%	59%	40%	43%
STAF	%mol	80.29	78.96	76.12	78.35	79.31	80.18	80.67	77.55	74.40	70.97	74.60	78.39	80.83	83.72	82.69	77.80	81.14	79.74	79.71	77.88
Surface Tension	N/m	0.346	0.344	0.358	0.347	0.342	0.343	0.339	0.347	0.341	0.369	0.359	0.354	0.343	0.350	0.334	0.352	0.338	0.343	0.343	0.354
Shear viscosity	log Pa s	4.91	*4.65*	*4.30*	*4.82*	*4.64*	4.96	4.90	4.59	4.53	3.821	4.568	4.586	4.59	4.916	4.89	4.43	4.82	4.65	4.82	4.64
Relative Viscosity	1	3.94	2.58	4.14	2.63	2.60	3.01	2.99	3.38	3.22	3.84	2.52	4.37	3.22	2.51	2.97	4.78	3.14	3.68	2.44	3.80
Effective Viscosity	log Pa s	5.50	5.06	4.91	5.24	5.05	5.44	5.37	5.12	5.04	4.41	4.97	5.23	5.10	5.32	5.36	5.11	5.31	5.21	5.20	5.22
Melt timescale	s	1.18	0.80	0.35	1.07	0.67	1.20	1.11	0.38	0.37	0.07	0.36	0.37	0.30	0.74					0.40	0.59
Bloating rate	1/min	0.0014	0.0074	0.0008	0.0063	0.0047	0.0007	0.0018	0.0003	0.0010	0.0012	0.0009	0.0030	0.0019	0.0030					0.0043	0.0015
Sintering rate	1/min	3.51	2.56	1.25	2.92	1.95	2.27	3.42	3.30	3.60	3.10	3.30	1.78	1.98	2.56					3.20	1.16
Start densification	°C	1036	928	985	946	942	991	990	971	952	949	954	957	1006	1035					961	969
Particle size	um	5.1	6.1	6.3	5.6	5.3	4.5	4.8	3.4	3.7	3.7	3.5	3.4	2.7	3.1					2.1	4.8

*$[Al_2O_3/(Al_2O_3+Na_2Oeq)*100]$

Table S3 (supplementary material)

Chemical composition, pseudo-structural parameters, and physical properties of the liquid phase. Sintering behaviour of porcelain stoneware.

		[39]		[33]				[35]		[18]						[32]			[44]	[15]	[41]
property	**unit**	**V0**	**V6**	**EG0**	**EAS3**	**ENS3**	**EQS3**	**C0**	**C6**	**NA**	**NAB**	**AT**	**ATP**	**NAK**	**K**	**W7**	**W12**	**W9**	**L20**	**G17**	**C17**
Firing temperature	°C	1220	1200	1200	1200	1180	1180	1200	1180	1200	1200	1200	1200	1200	1200	1185	1190	1185	1200	1230	1200
SiO_2	%wt	70.32	68.79	68.22	65.64	65.31	65.45	68.88	67.89	68.86	69.72	68.61	70.27	67.36	67.58	70.13	70.37	69.11	67.40	65.23	62.70
TiO_2	%wt	1.13	1.23	1.07	0.97	0.91	0.88	0.95	1.34	1.13	0.33	0.53	0.43	0.95	0.90	1.04	1.01	1.03	0.79	1.02	1.31
Al_2O_3	%wt	17.63	17.41	18.32	19.60	20.03	19.73	18.87	18.17	18.98	19.29	19.47	18.04	19.34	18.44	19.15	19.06	19.84	21.29	23.17	22.88
FeOtot	%wt	0.80	1.72	1.07	1.24	1.13	1.09	0.86	1.57	0.72	0.85	0.92	0.80	0.64	0.63	0.64	0.67	0.66	0.77	0.58	0.61
MgO	%wt	1.04	2.22	1.07	1.07	1.00	0.99	0.56	1.12	0.47	0.62	0.36	0.68	0.40	0.39	1.94	1.86	1.87	0.87	0.51	0.81
CaO	%wt	0.53	2.21	1.19	1.00	0.94	0.88	0.57	1.52	0.60	1.17	1.17	0.81	0.48	0.43	1.21	1.02	1.03	0.81	0.53	1.02
Na_2O	%wt	7.30	5.51	5.16	4.98	4.67	5.54	6.11	4.46	7.34	6.14	6.36	5.81	5.21	2.42	4.90	4.22	4.29	5.52	5.76	7.26
K_2O	%wt	1.25	0.91	3.90	5.50	6.01	5.45	3.21	3.93	1.90	1.89	2.59	3.17	5.62	9.22	0.99	1.79	2.17	2.56	3.19	3.39
others	%wt																				
Alumosity*	%wt	63.11	59.28	63.15	63.34	64.14	62.94	66.06	63.48	65.56	66.71	66.28	64.70	65.81	65.88	65.98	67.11	66.99	69.31	71.51	65.85
Solid load	1	0.368	0.360	0.329	0.302	0.355	0.311	0.342	0.523	0.362	0.310	0.327	0.284	0.295	0.301	0.323	0.304	0.301	0.319	0.430	0.284
NBOT	at	0.04	0.07	0.054	0.067	0.092	0.051	0.14	0.08	0.120	0.158	0.150	0.092	0.129	0.126	0.129	0.169	0.159	0.256	0.351	0.152
GNF	%at	40.3	39.9	40.5	40.3	40.3	40.3	40.1	40.1	39.9	39.9	40.0	40.8	40.6	41.3	39.3	39.4	39.1	38.82	38.11	38.73
Al fra GNF	%	18%	19%	21%	24%	24%	24%	20%	21%	18%	19%	20%	19%	22%	24%	17%	16%	17%	19%	20%	24%
GNM	%at	2.37	2.92	1.88	1.44	1.51	1.61	2.43	2.17	3.48	2.67	2.92	2.11	1.42	0.38	4.66	4.55	4.59	4.50	5.00	3.30
Al fra GNM	%	87%	62%	60%	53%	58%	39%	85%	79%	83%	87%	82%	77%	79%	0%	78%	80%	80%	88%	93%	82%
CCAT	%at	7.46	7.76	8.56	9.61	9.73	9.57	7.93	8.33	7.33	7.73	7.92	7.93	9.11	9.76	6.49	6.47	6.84	7.32	7.61	9.42
NaK fra CCAT	%	79%	50%	83%	86%	87%	80%	91%	59%	84%	91%	87%	88%	94%	97%	69%	71%	73%	85%	91%	87%
STAF	%mol	82.08	78.92	80.74	79.05	79.18	78.98	81.94	80.10	81.93	82.01	81.41	82.29	81.59	82.28	82.36	82.79	82.12	81.51	81.20	78.39
Surface Tension	N/m	0.336	0.349	0.337	0.336	0.338	0.338	0.336	0.341	0.338	0.342	0.340	0.336	0.331	0.322	0.357	0.354	0.354	0.342	0.346	0.346
Shear viscosity	log Pa s	4.64	4.60	4.8681	4.73518	4.95589	4.858418	4.94	5.08	4.86	4.90	4.87	4.93	5.00	5.27	5.0837	5.056	5.1895	4.91	4.69	4.64
Relative Viscosity	1	3.63	3.48	3.00	2.66	3.40	2.77	3.19	10.31	3.52	2.76	2.98	2.46	2.59	2.65	2.93	2.69	2.65	2.86	5.14	2.47
Effective Viscosity	log Pa s	5.20	5.14	5.34	5.16	5.49	5.30	5.44	6.10	5.41	5.34	5.35	5.32	5.41	5.69	5.55	5.49	5.61	5.37	5.40	5.03
Melt timescale	s	0.72	0.70	0.68	0.48	0.80	0.64	0.83	1.42	0.75	1.53	1.23	1.53	1.26	2.30						
Bloating rate	1/min	0.0002	0.0006	0.0019	0.0023	0.0019	0.0033	0.0020	0.0011	0.0006	0.0002	0.0003	0.0005	0.0006	0.0003						
Sintering rate	1/min	2.07	1.70	2.47	2.58	3.05	3.25	3.24	2.88	0.53	2.67	1.20	2.74	1.29	0.69						
Start densification	°C	1000	992	1030	994	971	967	985	950	1083	1067	1022	1091	1022	1122						
Particle size	um	5.5	6.1	3.1	3.0	3.0	3.0	3.2	4.0	3.5	6.6	5.6	6.0	4.2	4.0						

*[Al_2O_3/(Al_2O_3+Na_2Oeq)*100]

Table S3 (supplementary material)

Chemical composition, pseudo-structural parameters, and physical properties of the liquid phase. Sintering behaviour of porcelain stoneware.

		[42]									[38]			[26]	
property	**unit**	**CE**	**CO**	**IN**	**KD**	**KO**	**KT**	**LI**	**OS**	**RU**	**TaB**	**TaC**	**TaD**	**S15a**	**S15c**
Firing temperature	°C	1200	1200	1200	1200	1200	1200	1200	1200	1200	1220	1200	1200	1220	1220
SiO_2	%wt	66.54	68.70	67.89	69.06	66.84	66.32	68.11	66.48	65.21	73.40	73.84	71.07	69.09	63.88
TiO_2	%wt	0.74	0.72	0.74	0.48	0.93	0.74	1.06	1.09	1.35	1.22	0.92	0.82	0.80	0.79
Al_2O_3	%wt	19.97	17.72	18.37	18.38	20.39	20.42	18.86	20.31	21.44	15.61	14.67	16.82	19.04	21.60
FeOtot	%wt	1.25	1.27	1.23	1.34	0.85	1.78	1.22	1.26	1.16	0.69	0.85	1.56	1.07	0.74
MgO	%wt	0.04	0.07	0.02	0.01	0.02	0.02	0.03	0.02	0.04	0.29	0.62	0.71	1.62	0.32
CaO	%wt	2.77	2.55	2.76	2.06	2.11	2.04	2.62	3.69	3.61	0.91	0.73	0.89	2.38	4.75
Na_2O	%wt	5.23	5.42	5.81	6.47	6.93	6.28	4.80	5.87	5.62	6.53	6.11	6.15	5.13	4.75
K_2O	%wt	3.03	3.40	3.03	1.75	1.93	1.89	3.15	1.09	1.34	1.35	2.26	1.99	0.86	3.17
others	%wt														
Alumosity*	%wt	65.86	62.62	62.79	64.97	65.87	67.57	65.74	65.51	67.02	63.75	61.05	63.84	63.74	63.21
Solid load	1	0.408	0.391	0.419	0.328	0.379	0.370	0.373	0.477	0.458	0.252	0.266	0.230	0.383	0.396
NBOT	at	0.150	0.043	0.047	0.115	0.141	0.221	0.138	0.140	0.195	0.06	0.03	0.08	0.073	0.054
GNF	%at	39.51	40.82	40.55	40.01	39.51	38.69	39.91	38.98	38.37	41.1	41.8	40.5	39.50	39.60
Al fra GNF	%	21%	21%	22%	19%	21%	20%	20%	20%	21%	17%	17%	18%	18%	25%
GNM	%at	3.17	1.60	1.90	2.74	3.28	3.85	2.85	4.17	4.76	1.88	0.90	2.16	4.21	3.48
Al fra GNM	%	68%	42%	48%	73%	77%	81%	67%	68%	73%	78%	51%	75%	68%	49%
CCAT	%at	8.40	8.71	8.81	7.73	8.27	7.69	8.07	7.91	7.89	6.79	7.31	7.28	7.21	9.74
NaK fra CCAT	%	76%	79%	78%	81%	82%	81%	77%	67%	67%	88%	88%	85%	63%	63%
STAF	%mol	79.97	80.65	80.16	81.02	80.48	79.43	81.09	79.64	79.48	84.50	84.05	81.76	80.61	78.01
Surface Tension	N/m	0.343	0.337	0.339	0.341	0.344	0.345	0.340	0.350	0.352	0.330	0.330	0.336	0.348	0.349
Shear viscosity	log Pa s	4.90	4.94	4.87	4.87	4.83	4.78	5.08	4.85	4.86	5.04	5.12	4.91	4.61	4.53
Relative Viscosity	1	4.51	4.09	4.81	2.99	3.84	3.66	3.72	7.06	6.17	2.17	2.29	2.00	3.92	4.20
Effective Viscosity	log Pa s	5.56	5.55	5.55	5.35	5.42	5.34	5.65	5.70	5.65	5.38	5.48	5.21	5.21	5.16
Melt timescale	s										1.67	1.32	1.01		
Bloating rate	1/min										0.0011	0.0010			
Sintering rate	1/min										2.83	2.56	2.89		
Start densification	°C										990	987	985		
Particle size	um										5.0	3.3	4.2		

*$[Al_2O_3/(Al_2O_3+Na_2Oeq)*100]$

Table S3 (supplementary material)

Chemical composition, pseudo-structural parameters, and physical properties of the liquid phase. Sintering behaviour of porcelain stoneware.

		unpublished												
property	**unit**	**C**	**E**	**V0**	**GF5**	**GF9**	**GR**	**G1**	**G2**	**GPOR**	**AM**	**FW**	**P2**	**P4**
Firing temperature	**°C**	**1200**	**1200**	**1220**	**1200**	**1200**	**1200**	**1210**	**1220**	**1200**	**1200**	**1220**	**1200**	**1220**
SiO_2	%wt	68.45	68.08	69.43	61.40	60.38	61.09	62.38	62.80	72.27	66.08	62.92	65.54	65.79
TiO_2	%wt	0.75	0.55	1.10	1.05	0.79	1.30	1.37	1.22	0.85	1.05	0.50	1.26	1.53
Al_2O_3	%wt	16.70	16.92	19.88	21.57	23.28	24.34	24.76	22.97	18.51	20.78	23.67	21.60	21.11
FeOtot	%wt	2.18	1.80	0.70	4.55	4.01	1.96	1.18	2.26	0.65	0.97	0.46	1.41	1.77
MgO	%wt	0.83	0.57	0.10	2.10	1.75	1.24	1.07	1.14	0.83	0.37	0.29	0.67	0.69
CaO	%wt	1.33	0.75	0.30	1.39	1.55	1.35	1.53	2.42	0.01	1.08	0.88	1.17	1.29
Na_2O	%wt	4.76	5.89	6.39	5.38	5.05	4.26	4.13	4.24	5.77	7.14	6.22	4.46	4.08
K_2O	%wt	4.85	5.32	2.10	2.52	3.15	4.29	3.53	2.75	1.16	2.53	1.62	3.86	3.66
others	%wt													
Alumosity*	%wt	60.95	60.38	70.65	64.63	66.88	69.90	71.65	68.66	70.42	66.53	73.12	69.88	70.16
Solid load	1	0.479	0.426	0.318	0.356	0.239	0.391	0.317	0.342	0.339	0.359	0.289	0.350	0.327
NBOT	at	0.063	0.061	0.275	0.203	0.285	0.36	0.40	0.27	0.24	0.16	0.42	0.298	0.310
GNF	%at	40.8	40.8	39.21	40.2	40.6	37.1	36.9	38.6	39.5	41.0	37.5	38.4	38.2
Al fra GNF	%	22%	22%	17%	19%	20%	23%	21%	21%	14%	24%	19%	20%	20%
GNM	%at	0.81	0.80	3.90	2.48	2.04	5.32	6.25	4.06	4.32	1.57	6.39	4.29	4.40
Al fra GNM	%	0%	0%	96%	0%	0%	84%	86%	84%	94%	100%	94%	85%	84%
CCAT	%at	8.84	8.95	6.76	7.64	8.31	8.45	7.74	7.94	5.72	9.74	7.00	7.78	7.48
NaK fra CCAT	%	86%	98%	96%	77%	73%	80%	77%	83%	92%	74%	88%	84%	81%
STAF	%mol	79.21	79.33	83.40	71.82	72.26	76.62	78.79	76.80	84.64	80.03	81.19	80.14	80.01
Surface Tension	N/m	0.333	0.329	0.336	0.356	0.357	0.353	0.353	0.353	0.339	0.344	0.349	0.344	0.344
Shear viscosity	log Pa s	4.76	4.64	4.96	3.96	4.04	4.59	4.67	4.37	5.20	4.75	4.69	4.95	4.81
Relative Viscosity	1	7.17	5.01	2.85	3.41	2.07	4.09	2.84	3.18	3.14	3.46	2.52	3.31	2.97
Effective Viscosity	log Pa s	5.61	5.34	5.41	4.50	4.36	5.20	5.12	4.87	5.70	5.29	5.09	5.47	5.28
Melt timescale	s						0.66	0.79	0.53	1.27	0.72	0.63	0.98	0.68
Bloating rate	1/min				0.0012	0.0007	0.0018				0.0011	0.0017	0.0002	0.0007
Sintering rate	1/min				3.70	3.59	1.52	2.50	2.12	1.69	2.11	3.69	2.14	2.71
Start densification	°C				973	980	945	956	910	993	994	995	1009	991
Particle size	um				3.3	4.1	6.0	6.0	8.0	2.7	4.4	4.5	3.8	3.7

*$[Al_2O_3/(Al_2O_3+Na_2Oeq)*100]$

Figure 1S (supplementary material)
Graphical results of Rietveld refinement for sample V6 [39] fired at 1200 °C.
Goodness-of-fit statistics: Rp (%) 4.5; Rwp(%) 5.8; CHI**2 1.7

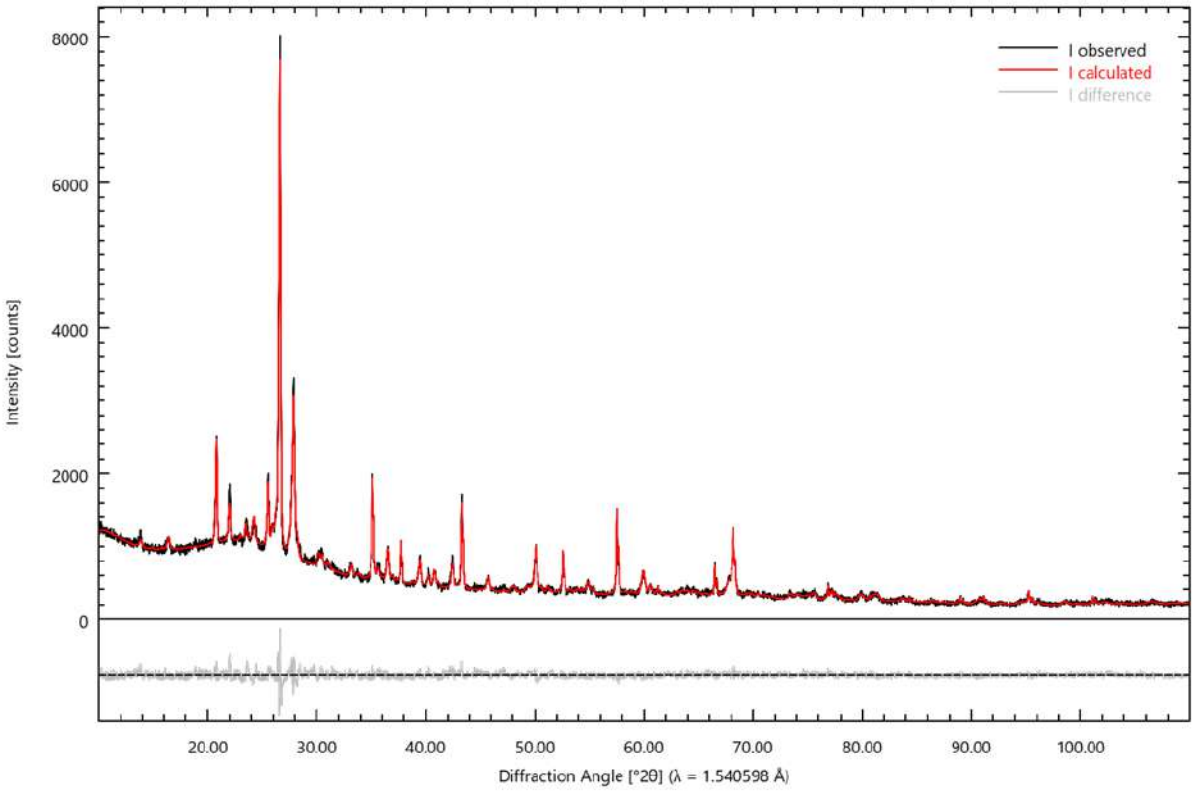

Figure 2S (supplementary material)
Methods followed for calculation of parameters used in data interpretation: Sintering behaviour

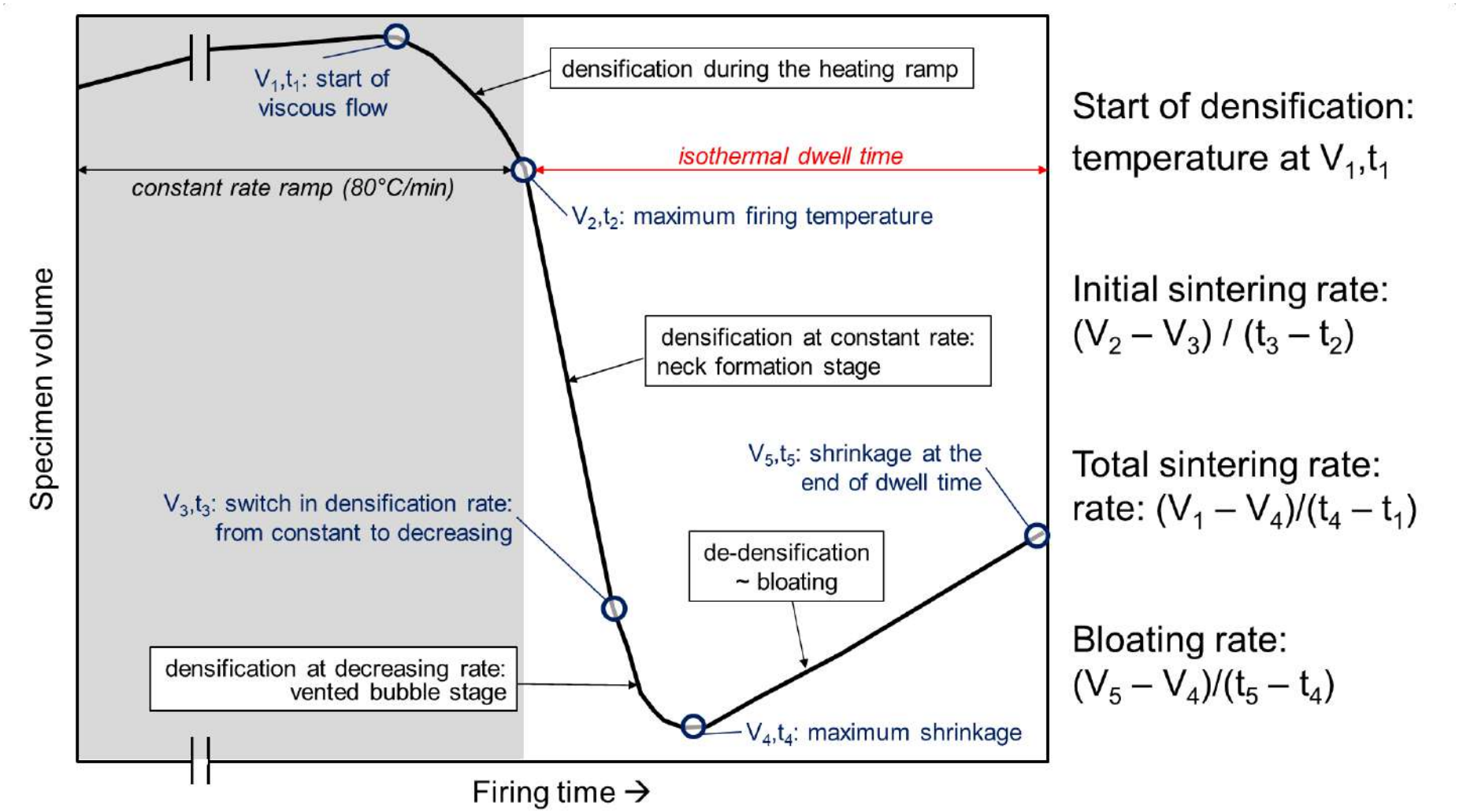

Figure 3S (supplementary material)
Trends of mullite, feldspars and vitreous phase as a function of alumosity and quartz as a function of silica content

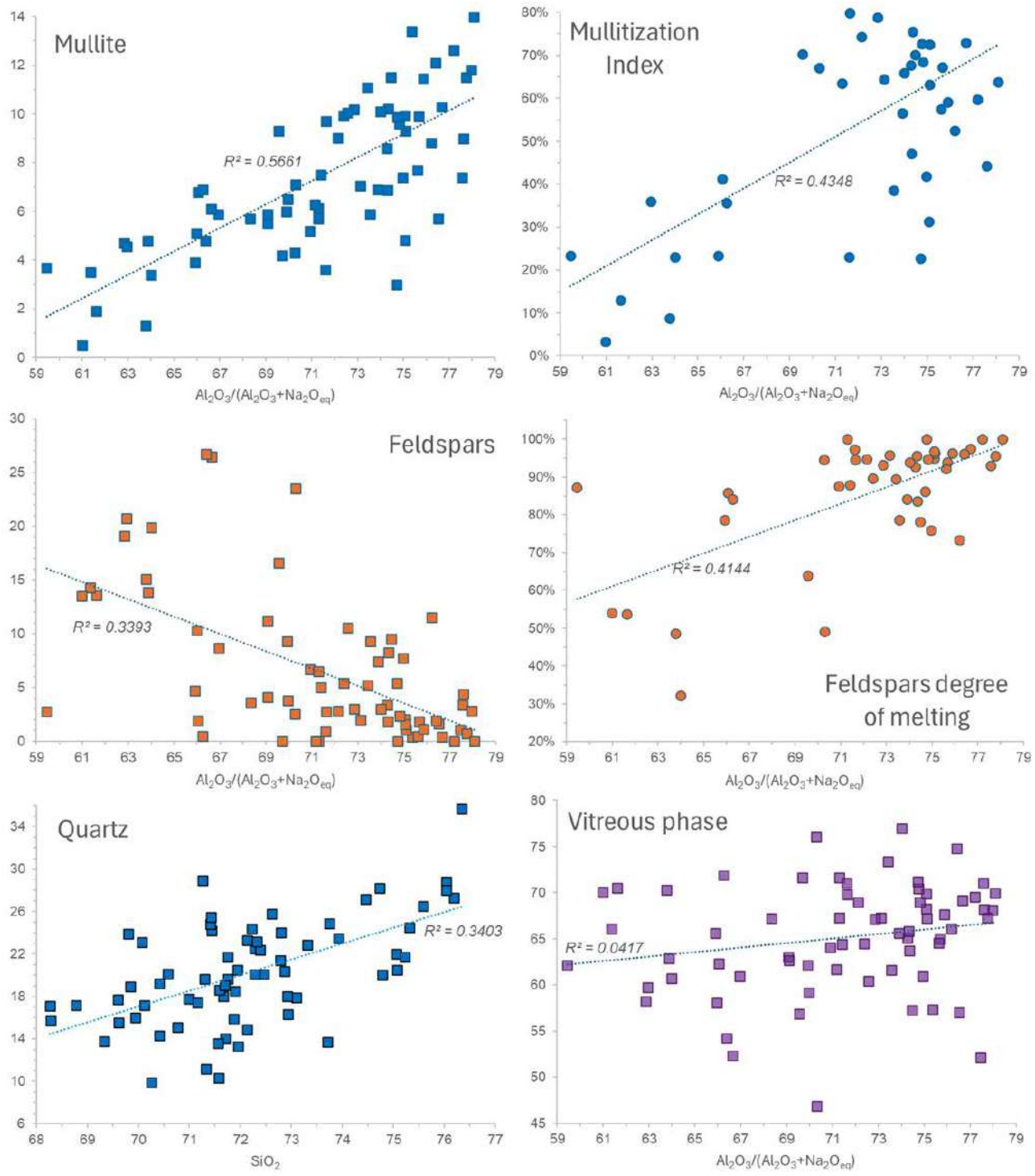

Figure 4S (supplementary material)
Shear viscosity of peraluminous silicate melts (SiO_2 content 67%) as a function of temperature and alumosity
Comparison with estimated viscosity of melts formed during the firing of porcelain stoneware